

**The X-ray spectra and spectral variability of intermediate type
Seyfert galaxies: *ASCA* observations of NGC 4388 and
ESO 103–G35**

Karl Forster ^{1,2}, Karen M. Leighly ¹, and Laura E. Kay ³

¹ Dept. of Astronomy, Columbia University, 550 West 120th Street, New York, NY 10027

² Current address: Harvard-Smithsonian Center for Astrophysics, 60 Garden Street,
Cambridge, MA 02138

³ Barnard College, Dept. of Physics & Astronomy, 3009 Broadway, New York, NY 10027

Electronic mail: kforster@head-cfa.harvard.edu

Submitted to the Astrophysical Journal

Received 29th January 1999; accepted 5th March 1999

ABSTRACT

The X-ray spectra of two intermediate type Seyfert galaxies are investigated using *ASCA* observations separated by more than a year. Both NGC 4388 and ESO 103–G35 exhibit strong, narrow Fe K α line emission and absorption by cold neutral gas with a column density $\sim 10^{23}$ cm $^{-2}$, characteristic of the X-ray spectra of type 2 Seyfert galaxies. The power law continuum flux has changed by a factor of 2 over a time-scale of ~ 2 years for both objects, declining in the case of NGC 4388 and rising in ESO 103–G35.

No variation was observed in the equivalent width of the Fe K α line in the spectra of NGC 4388, implying that the line flux declined with the continuum. We find that the strength of the line cannot be accounted for by fluorescence in line-of-sight material with the measured column density unless a ‘leaky-absorber’ model of the type favored for IRAS 04575–7537 is employed.

The equivalent width of the Fe K α emission line is seen to decrease between the observations of ESO 103–G35 while the continuum flux increased. The 1996 observation of ESO 103–G35 can also be fitted with an absorption edge at 7.4 ± 0.2 keV due to partially ionized iron, and when an ionized absorber model is fitted to the data it is found that the equivalent column of neutral hydrogen rises to 3.5×10^{23} cm $^{-2}$. The Fe K α line flux can be accounted by fluorescence in this material alone and this model is also a good representation of the 1988 and 1991 *Ginga* observations. There is then no requirement for a reflection component in the *ASCA* spectra of ESO 103–G35 or NGC 4388.

Subject headings: galaxies: active — galaxies: Seyfert — quasars: individual (NGC 4388, ESO 103–G35) — X-rays: galaxies

1. Introduction

The taxonomy of Seyfert galaxies has expanded from the straightforward types 1 and 2 classification to include various intermediate (1.2, 1.5, 1.8, and 1.9) types as well as type 3 or LINERS (Heckman 1980; Filippenko 1996). This system is primarily based on the strength of the broad permitted emission lines of the Balmer series which are broad compared to the width of the emission lines from forbidden atomic transitions such as $[\text{O III}]\lambda 5007$. There are now reasons to believe that what we are seeing is the result of a viewing angle dependence of optically thick material that obscures the Broad Emission line Region (BLR) formed in a toroidal distribution. The observation of broad Balmer lines in the polarized optical spectra, broad infrared emission lines of the Paschen series, and the large column densities measured in the X-ray spectra of some type 2 Seyferts lend support to what has become a unified model of Seyfert galaxies.

X-ray observations give a direct measure of the column density of line-of-sight material absorbing the continuum emission of the AGN. Comparison between the variations of the hard X-ray continuum and the $\text{Fe K}\alpha$ fluorescence emission line, produced by the transmission of X-rays through the absorbing material, allow an estimate of the location of the torus to be made. An example of this was seen in the X-ray observations of the type 1.9 Seyfert galaxy NGC 2992 (Weaver et al. 1996) which showed a delay between the $\text{Fe K}\alpha$ emission line strength and the declining 2 – 10 keV continuum.

The comparison of the equivalent width of the $\text{Fe K}\alpha$ emission lines to the measured column density in a sample of narrow line AGN (both type 2 and NELG \equiv type 1.8 and 1.9) observed by *ASCA* has shown that reprocessing by reflection and scattering can be also important (Turner et al. 1997ab; 1998). However these measurements did not indicate a location for the absorbing or reflecting medium because only a single epoch observation was presented for each object. Examination of the long term variation in the hard X-ray

(2 – 10 keV) flux from type 2 Seyfert galaxies has shown that changes by a factor of 2 – 3 are not unusual (Ueno 1997) and so we may observe a delay in the response of the Fe K α line to changes in the direct continuum.

Here we present multiple X-ray observations of two narrow line AGN, the type 1.9/2 Seyfert galaxy NGC 4388 and the type 1.9 Seyfert galaxy ESO 103–G35, to search for evidence of variations in the absorbing column, the 0.5 – 10 keV X-ray flux and Fe K α emission line over a period of ~ 2 years.

1.1. NGC 4388

The first type 2 Seyfert galaxy to be unambiguously detected in hard X-rays was NGC 4388, a nearly edge on spiral galaxy ($i \sim 72^\circ$, SB(s)b pec), that is the dominant source of hard X-rays in the Virgo cluster (Helou et al. 1981; Hanson et al. 1990; Takano & Koyama 1991). The low spectral resolution of the *SL2* XRT and *Ginga* LAC observations did not allow for a firm detection of any emission features in the spectrum of NGC 4388. The *SL2* spectrum of NGC 4388 could be modeled as a fairly flat ($\Gamma \simeq 1.5_{-0.5}^{+0.9}$) power law continuum absorbed by a large column density of cold gas ($N_{\text{H}} = 2.1_{-1.4}^{+2.8} \times 10^{23} \text{ cm}^{-2}$; Hanson et al. 1990). The H α /H β emission line ratio of the nuclear emission implies an extinction of $A_{\text{V}} \sim 1$ to 1.5, equivalent to a column $N_{\text{H}} = 5 \times 10^{21} \text{ cm}^{-2}$ (assuming a standard gas to dust ratio). Infrared spectroscopy has also revealed a strong 9.7 μm absorption feature in the spectrum of the nucleus of NGC 4388 consistent with the presence of large amounts of obscuring material (Roche et al. 1991).

High resolution spectra of the nuclear emission shows evidence of broad H α emission (FWZI $\sim 6000 \text{ km s}^{-1}$, Filippenko & Sargent 1985) although at a much weaker level than that claimed by Stauffer (1982). This, along with the detection of broad H α emission

from a region a few kpc from the nucleus (Shields & Filippenko 1988; 1996), results in a re-classification of NGC 4388 as an intermediate type 1.9 Seyfert galaxy. However, no broad $\text{Pa}\beta$ emission has been detected at either the nucleus of NGC 4388 (Ruiz, Rieke, & Schmidt 1994; Goodrich, Veilleux, & Hill 1994) or the off-nuclear position where broad $\text{H}\alpha$ was detected (Blanco, Ward, & Wright 1990). Spectropolarimetry of NGC 4388 has also failed to conclusively reveal broad emission lines in polarized light (Young et al. 1996) and the continuum polarization is low ($\sim 2\%$), most likely arising in dusty interstellar medium of the host galaxy (Kay 1994).

The Virgo cluster has been the target of a dozen observations by the *ASCA* satellite between 1993 and 1995, NGC 4388 appeared in the field of view of three of them. Here we present for the first time the result from a targeted observation of NGC 4388 taken in 1995. We also reanalyze one of the serendipitous 1993 observations previously reported by Iwasawa et al. (1997, hereafter I97). This is combined with a nearly simultaneous *ROSAT* PSPC observation to assist in the determination of the nature of the soft X-ray emission from NGC 4388. We also search for the presence of hard X-ray reprocessing by studying a *CGRO* OSSE observation taken 1 month after the 1993 *ROSAT* and *ASCA* observations.

1.2. ESO 103–G35

The *HEAO* A2 hard X-ray source 1H 1832–653 was identified with the S0/Sa type galaxy ESO 103–G35 ($z = 0.01329$) by Phillips et al. (1979) who classified the AGN as a type 1.9 Seyfert due to the weakness of the $\text{H}\beta$ emission line and the presence of a broad $\text{H}\alpha$ line with FWZI 6000 km s $^{-1}$. Examination of the ESO (B) atlas shows that the host galaxy has an inclination angle of $\sim 60^\circ$ (Kirkahos & Steiner 1990). A deep $9.7\mu\text{m}$ absorption feature implies a substantial optical depth at $10\mu\text{m}$ toward the emitting source (Roche et al. 1991) and ESO 103–G35 is also seen to host an H_2O megamaser (Braatz,

Wilson, & Henkel 1996). A large absorbing column ($N_{\text{H}} > 10^{23} \text{ cm}^{-2}$) was directly observed in *EXOSAT* and *Ginga* observations (Turner & Pounds 1989; Warwick et al. 1993).

The *EXOSAT* observations of ESO 103–G35 indicated a possible variation in the column density over a period of four months interpreted as due to motion of material in the BLR across the line-of-sight to the continuum source (Warwick, Pounds, & Turner 1988). We present three *ASCA* observations of ESO 103–G35; note however that the 1994 observation was previously reported in Turner et al. (1997a).

2. Observations

2.1. *ASCA*

The *ASCA* observations of NGC 4388 and ESO 103–G35 examined here were obtained from the HEASARC archives as well as proprietary data and analyzed using the XSELECT and XSPEC software packages (Arnaud 1996). Tables 1a and 1b give a log of the *ASCA* observations examined in this paper along with the screening criteria used to select useful events. Standard background cleaning was applied to remove events due to high-energy particles, and the light curves were examined for data dropout and periods of high background level. Hot and flickering pixels were removed from the Solid-state Imaging Spectrometer (SIS) data. The faint mode data were converted to BRIGHT2 mode after correction for dark frame error and echo effect.

The SIS detectors have suffered a steady degradation since launch due to the harsh radiation environment in orbit. There are two major effects, Residual Dark Distribution (RDD) and non-uniform Charge Transfer Inefficiency (CTI), both of which impair the CCD chips in the SIS instruments (see Dotani et al. 1995; 1996 for details). These effects can be corrected for in the extraction of the events from the detectors, but only the 1995

NGC 4388 and 1996 ESO 103–G35 data were corrected for RDD as the effect is not significant in observations taken before 1995. Note that only the 2-CCD mode data from the 1993 observation of NGC 4388 is examined here as the few events which we were able to extract from the 4-CCD mode data did not significantly improve the signal-to-noise ratio of the data.

NGC 4388 is in the field of view of both the Gas Imaging Spectrometer (GIS) and the SIS detectors in only one of the 1993 *ASCA* observations (of NGC 4374 on 4 July 1993, hereafter the 1993b observation) and this observation is examined in detail here. The distribution of X-ray events from NGC 4388 on the detectors during the remaining serendipitous observation (of NGC 4406 on 3 – 4 July 1993, hereafter the 1993a observation) is somewhat uncertain and the extreme off-axis position ($18'$) of NGC 4388 in the GIS 2 data and its proximity to the calibration source in the GIS 3 data may give spurious results. The choice of areas on the GIS and SIS detectors to represent an accurate background for the observations of NGC 4388 is problematic as this galaxy lies 1.3° from M87 and has two giant elliptical galaxies, NGC 4374 (M84) and NGC 4406 (M86), within $18'$. This creates a complicated mosaic of X-ray emission across the detectors and the extraction regions must be chosen with care to collect as many events due to the AGN as possible but also to account correctly for variations in the intensity of the background thermal X-ray emission that is known to exhibit a variety of temperatures (Takano et al. 1989; Awaki et al. 1994). For this reason the use of the *ASCA* blank sky observations for background regions is unsuitable even though NGC 4388 lies at high Galactic latitude ($l^{\text{II}} = 74^\circ$).

Although NGC 4388 is not a bright X-ray source, extraction regions $6'$ in radius were used, as recommended for GIS observations of bright point sources. The background extraction region was chosen to be an annulus around this circle out to a radius of $8'$, different from those employed by I97. However, we find that the background spectra from

the regions chosen by I97 and those used here are essentially identical. The extraction regions chosen for the SIS observations of NGC 4388 are polygons lying within the chip boundaries, approximating circular regions of radius $4'$ to $5'$ as recommended for SIS observations of point sources (Day et al. 1995). The background was taken from regions around the source extraction region out to the edge of the same chip but within a radius of $\sim 8'$. The standard technique for background subtraction of using regions around the edge of the same chip that the target is placed on was found not to be suitable for the observations of NGC 4388 due to the spatially variable nature of the soft X-ray emission from the Virgo cluster.

The radial profile of the X-ray emission from NGC 4388 was investigated in the *ASCA* observations in both soft X-ray (0.5 - 3.0 keV) and hard X-ray (3.0 - 10.0 keV) bands; however no indication of extended emission was found. This is not surprising as the emission observed in the 1991 *ROSAT* HRI observation that extends out to $40''$ (Matt et al. 1994) and the $2'$ X-ray lobe seen in the 1993 PSPC observation (Colbert et al. 1998) would be difficult to detect with the *ASCA* instruments providing $\lesssim 100$ total events above background during the observations.

ESO 103–G35 was observed by *ASCA* on three occasions, September 1994, September 1995, and March 1996 (see Table 1b). The standard extraction region of a circle with a radius $6'$ for the target events and an annulus out to $8'$ for the background events were used for the GIS observations of ESO 103–G35. For the SIS observations of ESO 103–G35 the target events were taken from circular regions of $4'$ radius centered on ESO 103–G35, except for the 1996 SIS 1 data which were extracted from a $8'.4 \times 7'.2$ box as ESO 103–G35 was too close to the edge of the chip for a circular extraction region to be used. Background events were taken from rectangular regions around the edge of the same chip with approximately the same area as the extraction regions, avoiding a regions closer than $\sim 5'.5$ to the target.

The radial profile of all the *ASCA* observations of ESO 103–G35 were consistent with a point source for events above 2 keV, there being too few events below that energy to make a useful comparison.

The data from the GIS and SIS instruments were rebinned so that each spectral channel contained at least 20 counts so that chi-square statistics are applicable for spectral fitting. Standard response files were used for the GIS data and response matrices were created for each SIS instrument. Ancillary files for both GIS and SIS data were also created using FTOOLS packages. Note that the GIS and SIS data (both 2 CCD and 4 CCD) are modeled simultaneously including a parameter needed to account for minor differences in the normalizations of the GIS and SIS instruments.

2.2. *ROSAT* PSPC

NGC 4388 has appeared in two *ROSAT* PSPC observations; however the first of these (the December 1991 observation of NGC 4406) placed NGC 4388 in a region on the detector shadowed by the PSPC window support structure and therefore this observation was not analyzed. It was fortunate that a targeted *ROSAT* PSPC observation of NGC 4388 was made during the 1993 *ASCA* observation. Combining the *ROSAT* and *ASCA* spectra extends the band pass to lower energies where the sensitivity of the *ASCA* instruments is rapidly declining. An analysis of the PSPC spectrum (Rush & Malkan 1996) and the image (Colbert et al. 1998) is available and so we shall only describe the results from a simultaneous fitting of the *ROSAT* and *ASCA* data (§3.8). The *ROSAT* PSPC data were extracted in the standard manner (Turner 1996) with periods of high background level excluded. The background subtracted count rate between 0.1 and 2.0 keV was 0.045 s^{-1} for a total exposure of 11.65 ks.

A *ROSAT* PSPC observation of ESO 103–G35 was performed between 31 March and 12 April 1993 (Colbert et al. 1998) with the target 4.′6 off-axis. A standard extraction aperture of radius 2.′5 was used. A nearby bright source was excluded from the background region, chosen to be an annulus of outer radius 4.′. The final exposure time, after excluding periods of high background, is 16.3 ks giving a 0.1 – 2.0 keV background subtracted count rate of $4.9 \times 10^{-3} \text{ s}^{-1}$. There are two faint point sources, with PSPC count rates of $\sim 0.03 \text{ s}^{-1}$, within 6′ of the position of ESO 103–G35 and these will have contaminated the soft X-ray events observed with the *ASCA* instruments. The PSPC spectra of these two sources can be fitted with a blackbody model of temperature 0.12 and 0.14 keV.

2.3. Short time-scale variability

The light curves of all the *ASCA* and *ROSAT* observations of NGC 4388 and ESO 103–G35 were examined for evidence of short term X-ray variability. No significant variability was observed in the background-subtracted events due to NGC 4388 during a 1.75 day *ROSAT* HRI observation in December 1991 or during the 1993 *ROSAT* PSPC observation that spanned 16 days. A comparison between GIS detector areas centered on the position of NGC 4388 and various regions on the detector during the 1993 *ASCA* observations showed no significant variability of events due to NGC 4388 sampled on time-scales from minutes to days. The X-ray events were also split into two broad energy bands but no variability was discovered in either the soft ($0.5 < E < 3.0 \text{ keV}$) or hard X-ray events ($3.0 < E < 10.0 \text{ keV}$) during the observations. The events from both the GIS and SIS instruments during the 1993b and 1995 observations were summed and the background events subtracted. The energy range of the events were also restricted to be above 2 keV, where the flux from the AGN dominates over the Virgo cluster emission, and below the energy where NGC 4388 is detected above the background level (10 keV for the

GIS and 9 keV for the SIS observations). The variations are statistically significant at the 99% level only for the 1995 observations; however the uncertainties in the count rates are large and the GIS and SIS detector variations do not match very well. Thus we cannot confirm that any variations in X-ray emission occurred on a time-scale of days during the *ROSAT* and *ASCA* observations of NGC 4388.

Statistically significant variations in count rate were observed during all the *ASCA* observations of ESO 103–G35. However we only claim significant variability for the 1996 observation where χ^2_ν (SIS) = 7.2 and χ^2_ν (GIS) = 5.5 ($\nu = 6$) compared to a constant source. In this observation the signal to noise is highest and the variations in count rate are similar in both the GIS and SIS detectors and so we present this light-curve in Figure 1.

3. Spectral Analysis

3.1. The *ASCA* spectra of NGC 4388

For each observation a number of different continuum models were applied to the data, and for each case the chi-square statistic of the goodness of fit along with the number of degrees of freedom in the model fit are quoted (the 1993b data followed by 1995). The F-test probability statistic (Bevington & Robinson 1992) is also quoted where different models are compared. An absorbed power law model (1PL) can be rejected for all the observations at $> 99.99\%$ level ($\chi^2/dof = 447.2/329; 873.2/541$). The residuals from this fit to the SIS data are presented in Figure 2. Immediately obvious in all the *ASCA* spectra is a strong emission line near 6.4 keV and a soft X-ray excess below 3 keV. The poor statistics seen in the spectra below 3 keV is a consequence of the subtraction of the high background flux from the Virgo cluster whose thermal spectrum peaks around 1 keV.

When the soft X-ray emission was modeled as an unabsorbed power law continuum

(2PL), it was found that the model fit improved significantly ($393.9/327$, $P_{\text{F-Test}}^{1993} \ll 0.001$; $629.0/539$, $P_{\text{F-Test}}^{1995} \ll 0.001$). No improvement was made over the 2PL model if instead a Raymond-Smith thermal plasma emission model (Raymond & Smith 1977) is added to an absorbed power law (RS+PL) to model the soft X-ray emission.

However the model used by I97 included both thermal emission and unabsorbed power law components (RS+2PL), and when this model is applied to the data the chi-square values of the residuals are significantly reduced in both observations ($\Delta\chi^2/\Delta dof$ 9.6/2; 25.0/2). When the photon indices of the power law components are then constrained to be the same, the model fit did not significantly degrade or improve. There was also no improvement when each continuum component was associated with a separate column of absorbing material and it was found that the columns absorbing the thermal and the (less absorbed) power law components were consistent with that found in the RS+2PL model. Models that included 2 thermal components (Raymond-Smith and Blackbody or 2 Raymond-Smith components) in addition to a heavily absorbed power law also provided a reasonable fit to the data ($396.7/322$; $641.7/534$). However the temperature of the second thermal component was ~ 10 keV and could not be constrained and so we rejected this model.

We agree then with I97 that the RS+2PL model proves a satisfactory description of the continuum emission seen in the *ASCA* observations of NGC 4388. The addition of a Gaussian emission feature near 6.4 keV also improves upon the RS+2PL model fit significantly ($320.6/321$ $P_{\text{F-Test}}^{1993} \ll 0.001$; $542.3/533$ $P_{\text{F-Test}}^{1995} \ll 0.001$) for both observations and will be discussed in §3.4 below. Table 2a presents the RS+2PL models along with the 90% error estimate for 4 Interesting Parameters (IP). These models, unfolded from the instrumental response, are shown in Figure 3 along with the ratio of the data to the folded model. The confidence contours for the parameters in the RS+2PL models fitted

simultaneously to the SIS and GIS data in each observation are presented in Figure 4, where the contour levels are $\Delta\chi^2$ at 68%, 90%, and 99% levels for 4 IP ($\Delta\chi^2$ 4.72, 7.78, and 13.3 respectively) except for Fig. 4f where the contours are $\Delta\chi^2$ for 2IP. This is a departure from the standard reporting of error estimates for modeling of X-ray spectra where errors based on 1 or 2 IP are usually quoted. However, in complicated, multi-component models, each continuum model parameter is sensitive to changes in other parameters and so the $\Delta\chi^2$ values of more IP should be quoted to give a more legitimate estimate of the errors in the model (Yaqoob 1998). As an example, the error estimate for the photon index includes the photon index, the normalizations of both power law components and the absorbing column as interesting parameters, the other parameters being frozen at their best fit values.

The total fluxes between 0.5 and 10.0 keV for these models are $f_X = (1.42, 0.68) \times 10^{-11}$ ergs cm $^{-2}$ s $^{-1}$ (1993, 1995 respectively). The power law continuum models shown in Table 2a give an absorption corrected 2 – 10 keV luminosity for NGC 4388 of $L_X = (2.78, 1.28) \times 10^{42}$ ergs s $^{-1}$ (1993, 1995 respectively) for a distance to the Virgo cluster of 27 Mpc (Fabbiano, Kim, & Trinchieri 1992).

3.2. The *ASCA* spectra of ESO 103–G35

The residuals from fitting an absorbed power law to the *ASCA* observations of ESO 103–G35 are presented in Figure 5. Residuals around 6 keV and below 3 keV can be seen and there is also a feature near 0.9 keV in the 1994 and 1996 data that may be an emission line, or blend of lines. The absorbed power law model is a poor description of the observations; the χ^2/dof for 1994, 1995 and 1996 respectively are 320.2/280, 105.9/98 and 615.6/532. The addition of a Gaussian emission line near 6.4 keV to the absorbed power law significantly improves the fit in all the observations (274.7/277, 82.8/95 and 575.6/529; $P_{F-Test}^{1994} < 0.001$, $0.01 < P_{F-Test}^{1995} < 0.001$ and $P_{F-Test}^{1996} < 0.001$) and is discussed in detail

below (§3.4). A significant improvement is made in the 1994 and 1996 observations when the soft X-ray residuals are accounted for with the addition of a second (less absorbed) power law (262.7/275, $0.02 < P_{\text{F-test}}^{1994} < 0.01$ and 534.0/527, $P_{\text{F-test}}^{1996} < 0.001$) There are very few soft X-ray counts in the 1995 observation and so the improvement in adding a second power law is not significant (78.2/93, $0.2 < P_{\text{F-test}}^{1995} < 0.1$) but for consistency we include the second power law in the analysis of the 1995 observation.

The contaminating sources seen in the *ROSAT* PSPC observation (§2.2) should have provided at least twice as many soft X-ray events than those observed during the *ASCA* observations. One of these sources can be identified with a $m_{\text{B}} = 11.5$ star with a proper motion of $\mu = 0.165 \pm 0.022$ arcsec yr⁻¹ (Wroblewski & Torres 1994), and the other remains unidentified. The flux from the PSPC observation of the weak, unresolved nuclear soft X-ray source identified with ESO 103–G35 is consistent with that seen during the 1994 *ASCA* observation, although slightly low compared to that observed in the 1996 observation. There are so few soft X-ray events accumulated during the *ASCA* observations that a model that combines thermal and power law emission to describe the flux below 2.5 keV does not allow the parameters to be meaningfully constrained. A model where the flux below 3 keV is due to thermal emission alone does not improve on the two power law model (261.3/273, 77.7/91 and 535.3/525) and the low signal to noise does not allow a good constraint of the temperature of this component to be made (e.g. kT (1994) $\lesssim 1.9$ keV). We therefore parameterize the soft X-ray emission with a power law alone noting that a proportion of the flux may be due to contaminating sources.

The parameters for the two power law plus Gaussian emission line model are presented in Table 2b, the model unfolded from the instrumental response and the data to model ratio are shown in Figure 6, and the χ^2 confidence contours of the model fitted simultaneously to the GIS and SIS data in each observation are shown in Figure 7. The total 2 – 10 keV

flux is $f_X = (1.42, 2.43, 2.41) \times 10^{-11}$ ergs cm $^{-2}$ s $^{-1}$ (1994, 1995, 1996 respectively). The absorption-corrected 2 – 10 keV luminosity of ESO 103–G35 calculated from the power law parameters is found to be $L_X = (2.62, 3.11, 4.73) \times 10^{43}$ ergs s $^{-1}$ (1994, 1995, 1996 respectively) for a redshift of $z = 0.01329$ assuming $H_0 = 50$ km s $^{-1}$ Mpc $^{-1}$ and $q_0 = 0.5$.

3.3. Fe K edge

The possibility of ‘excess’ absorption at 7 keV, i.e. more than that required for the measured absorbing column, was investigated. A model with absorption by neutral material of Solar metallicity was applied to the data but with the Fe abundance set to zero in order to measure the strength of the absorption edge. It was found that the presence of an edge due to *neutral* iron (near 7 keV) is required (i.e. significantly improves the model fit) in all the *ASCA* observations of NGC 4388 and ESO 103–G35. The optical depth of the edge in the observations of NGC 4388 was found to be $\tau_{93} = 0.42^{+0.36}_{-0.26}$ at $E_{93}^{\text{edge}} = 7.26^{+0.39}_{-0.41}$ keV and $\tau_{95} = 0.54^{+0.35}_{-0.27}$ with $E_{95}^{\text{edge}} = 7.31^{+0.68}_{-0.53}$ keV. For the 1994 observation of ESO 103–G35 we find $E_{\text{edge}} = 7.09 < 8.0$ keV and $\tau = 0.16 (< 0.35)$. Note that the errors quoted for the absorption edge parameters are 90% confidence for **2 IP**. The confidence contours for the absorption edge parameters are presented in Figure 8 and are consistent with no change in the optical depth between the observations of NGC 4388.

The exception is the 1996 observation of ESO 103–G35. This spectrum can be fitted with an edge at $7.37^{+0.26}_{-0.22}$ keV (errors are 90% confidence for 4 IP) with an optical depth of $\tau = 0.47^{+0.16}_{-0.12}$. This model is a marginally significant improvement over the neutral absorption edge model ($\Delta\chi^2/\Delta\text{dof} = 8.86/2$) and is not an artifact of the systematics in the data as the feature is significant in all 4 detectors. This absorption edge is consistent with that seen in the 1988 *Ginga* observation of ESO 103–G35 (Warwick et al. 1993). The energy of the edge feature implies that a significant proportion of the iron is in an ionization

state between Fe IX and Fe XVII. Models of the ionization structure of photoionized gas in this ionization state imply that the ionization parameter (ξ), which can be thought of as the ratio of ionizing photons to the density of the absorbing material, is in the range $25 \lesssim \xi \lesssim 320$ (Kallman & McCray 1982). When the 1996 observation is modeled with absorption by ionized material (XSPEC absori model) it was found that the absorption column rose to $N_{\text{H}} = 3.5 \pm 0.3 \times 10^{23} \text{ cm}^2$, with an ionization parameter of $\xi = 83^{+40}_{-74}$, and Fe abundance $Z_{\text{Fe}} = 0.97^{+0.71}_{-0.52} Z_{\odot}$ ($\Delta\chi^2/\Delta dof = 6.5/2$ compared to the model of absorption by neutral material). This column agrees with the measured optical depth of the ionized Fe K α edge. Note that the position of the Fe K α emission line is near the neutral value which is expected for this ionization state. The peak energy does not move to a significantly higher energy until ionization state $\sim \text{Fe}^{19+}$ is reached. The effect of resonant trapping opacity will reduce the number of Fe K α line photons in material with an ionization parameter in the range $100 \lesssim \xi \lesssim 500$ but is not a significant effect for $\xi \lesssim 100$ and so will have little effect here (Matt, Fabian, & Ross 1993). The confidence contours for the absorption edge parameters are shown in Fig. 8 where it can be seen that the 1996 edge is stronger than that observed in the 1994 observation. The 1994 data cannot distinguish between a neutral or ionized absorption edge whereas a neutral Fe K edge can be excluded from the 1996 observation at the 99% confidence level.

It is possible that only a proportion of the gas along the line of sight to the continuum source is in a non-neutral state. If we apply a dual absorber model to the 1996 observation of ESO 103–G35, with a neutral and an ionized column, we find that the ionization parameter rises to $\xi = 290^{+850}_{-260}$ with absorbing columns are $N_{\text{H}}^{\text{Cold}} = (1.1^{+0.8}_{-0.7}) \times 10^{23} \text{ cm}^{-2}$ and $N_{\text{H}}^{\text{Ionized}} = (1.7^{+1.3}_{-1.4}) \times 10^{23} \text{ cm}^{-2}$. The improvement over the model fit given in Table 2b (2PL) is not significant ($\Delta\chi^2/dof = 0.1/1$). The errors quoted here are 90% confidence for 2IP, and these parameters are not well constrained so we do not explore this model any further.

Material with a high ionization parameter may produce recombination features around 1 keV (Netzer 1996; Matt, Brandt, & Fabian 1996) and there do appear to be residuals near 1 keV in the spectrum of ESO 103–G35 shown in Fig. 5. Similar features appear in the *ASCA* spectra of Mkn 3 and NGC 4507 and are attributed to hydrogen-like oxygen and helium-like neon respectively (Griffiths et al. 1998; Comastri et al. 1998). In the reflection-dominated X-ray spectra seen in a few type 2 Seyfert galaxies such as Circinus (Matt et al. 1996) and NGC 6552 (Reynolds et al. 1994), emission lines in the *ASCA* bandpass are expected to be strong and can provide a measure of the ionization parameter and abundance in the scattering medium (Netzer, Turner, & George 1998). To test the significance of these features a Gaussian emission feature was added to the models in Table 2b; however in neither the 1994 or 1996 spectra does the addition of a Gaussian emission feature significantly improve the model fit (1994 $\Delta\chi^2/dof = 1.4/3$; 1996 $\Delta\chi^2/dof = 2.5/3$).

3.4. Fe $K\alpha$ emission line

The results of adding a single Gaussian line to the power law continuum to account for the the strong emission feature near 6.4 keV in the *ASCA* spectra of NGC 4388 and ESO 103–G35 can be found in Tables 2a and 2b. A single, narrow, Gaussian proves to be a reasonable description of the emission feature in all of the spectra; note that the rest-frame values for line peak energy are quoted. The improvement in the χ^2 residuals of adding a Gaussian line were highly significant in all the observations. The confidence contours of the emission line parameters are shown in Figs. 4 & 7 where it can be seen that the line is marginally resolved (at the 1σ level) in the 1993 NGC 4388 and 1994 ESO 103–G35 spectra. In the other observations the line remains unresolved.

The peak of the emission line in all of the observations is consistent with an identification with neutral to partially ionized Fe $K\alpha$ (up to ionization state Fe XIX,

Turner et al. 1992). The branching ratios demand that Fe K β fluorescence be produced at a level 0.135 relative to Fe K α (Leahy & Creighton 1993) and lines of this strength were searched for near 7.085 keV (rest frame). The addition of a line of the correct relative strength and peak energy resulted in a reduction in χ^2 in all but the 1995 spectrum of ESO 103–G35 where no emission feature at the correct energy could be found ($\Delta\chi^2/\Delta dof$ for NGC 4388 — 1993 = 1.6/2, 1995 = 0.3/2; ESO 103–G35 — 1994 = 2.09/1, 1995 = 0.47/3, 1996 = 4.0/1). However, only in the 1996 observation of ESO 103–G35 were these improvements statistically significant.

When the parameters of the second Gaussian emission were left free it was found that the 1993 SIS spectrum of NGC 4388 could be fitted with an additional narrow line centered at 7.02 keV. However the model fit was not a significant improvement over the use of a single Gaussian ($\Delta\chi^2/\Delta dof = 1.6/2$). The 1995 observation of NGC 4388 could also be fitted with two narrow ($\sigma = 0.0$ keV) Gaussians at 6.35 keV and 6.42 keV that mimic the single broader, but unresolved line, with no improvement in the model fit ($\Delta\chi^2/\Delta dof = 0.1/3$). The residuals in the 1996 SIS observations of ESO 103–G35 also suggest the presence of a second line at ~ 7.0 keV (rest frame), although there is no significant improvement to the fit when a second line is added ($\Delta\chi^2/\Delta dof = 0.3/3$).

3.5. Dual absorption models

A version of the dual absorber model (Weaver et al. 1994) is the ‘leaky-total absorber’ favored for the X-ray spectrum of IRAS 04575–7537 (Vignali et al. 1998). In this type 2 Seyfert galaxy the measured absorbing column is an order of magnitude too small to account for the strength of the Fe K α emission line. An absorber with $N_{\text{H}} \sim 10^{23} \text{ cm}^{-2}$ covering 36% of the continuum source was invoked to explain both the flat continuum and the strength of the Fe K α emission line in IRAS 04575–7537. Complimentary evidence for

a larger absorbing column in IRAS 04575–7537 is the large optical depth of the Fe K edge ($\tau_{\text{FeK}} = 0.33^{+0.14}_{-0.13}$). Such a dual absorber model may be relevant for the X-ray spectrum of NGC 4388 because the strength of the Fe K α emission line implies an absorbing column $N_{\text{H}} \sim 10^{24.5} \text{ cm}^{-2}$ leading to large optical depth for the Fe K edge ($\tau > 1.0$). If a similar leaky-absorber model is applied to the *ASCA* observations of NGC 4388 no significant improvement is made over the RS+2PL model. However the power law becomes closer to the $\Gamma \simeq 1.9$ value associated with unified models (see §3.6) and the larger absorbing column can help to explain the strength of the Fe K α line. We present the model parameters in Table 3 and shall discuss this in §4.2 as this model appears to be a reasonable choice for the X-ray spectrum of NGC 4388.

For the observations of ESO 103–G35 however, the parameters for a leaky-absorber model were very poorly constrained even at the 1σ level. The model does not improve on the simpler single absorbing column model and the covering fraction is found to be low ($< 20\%$) and so we do not investigate this model further.

3.6. Compton reflection

The hard X-ray spectra of many type 1 Seyfert galaxies exhibit a ‘Compton reflection hump’ in the 20 – 100 keV band, expected when X-ray irradiation of cold ($T < 10^6 \text{ K}$) matter with a high covering fraction occurs (Lightman & White 1988; George & Fabian 1991; Nandra & Pounds 1994). An investigation of the *Ginga* spectra of Seyfert galaxies found that the effects of a reflection component can be important below 20 keV and this has led to a modification of the so called “canonical” X-ray power law slope from $\Gamma \equiv 1.7$ (Turner & Pounds 1989) to $\Gamma \equiv 1.9$ when the reflection continuum is taken into account (Nandra & Pounds 1994). More recently, observations above 50 keV have shown that a Compton reflection component is present in the average spectrum of Seyfert galaxies, with

very little difference seen between the hard X-ray spectra of type 1 and type 2 Seyfert galaxies (Zdziarski et al. 1995).

We searched for the presence of a reflected continuum from both neutral and/or ionized material in the observations of NGC 4388 and ESO 103–G35. In all the observations the model fit was not significantly improved by using a reflection model. This was also found to be the case when the second (\sim unabsorbed) power law component was modeled as a reflection continuum ‘leaking’ through lower column density material. However, these model fits were also not significantly worse than the power law models, and so cannot be ruled out on statistical grounds alone. The power law slopes of the reflection model fits were in general steeper than for the RS+2PL and 2PL models but within the error estimates for these models (Tables 2ab). We do not include the details of the models here because the parameters of the reflection components are poorly constrained. The relative contribution of a reflected continuum was examined in the observations but no significant changes between the observations could be determined. The difficulty in determining whether a significant level of X-ray reflection is present is not only associated with the problem of measuring the power law slope when the continuum is heavily absorbed but also to the limit of *ASCA* detector sensitivity to $\lesssim 10$ keV.

Fortunately, an Oriented Scintillation Spectrometer Experiment (OSSE) observation of NGC 4388 was made between 25 August and 6 September 1993 and this allows spectral modeling from 0.1 keV to 1000 keV when combined with the *ROSAT* and *ASCA* observations taken 1 month previously. OSSE is one of the instruments aboard the *Compton Gamma Ray Observatory* (see Johnson et al. 1993 for a detailed description of the OSSE experiment, performance and data analysis procedures). There was also a 1992 OSSE observation of NGC 4388 that observed a flux density of $(6.35 \pm 0.58) \times 10^{-6}$ photons $\text{cm}^{-2} \text{ s}^{-1} \text{ keV}^{-1}$ at 70 keV and a spectral slope of 2.37 ± 0.22 (Kurfess 1994; Johnson

et al. 1994). The steepness of the observed soft gamma-ray slope is typical for radio-quiet Seyfert galaxies and can be modeled as an exponential cutoff in the hard X-ray power law continuum. A comparison between the 1992 and 1993 OSSE observations found no significant flux or spectral variability. The OSSE data is difficult to interpret due to the proximity of M87 and because of this the background is taken from only one side of the offset pointings. The 1993 observations of NGC 4388 are presented in Figure 9, along with the model of the simultaneous fit to the *ROSAT* PSPC and *ASCA* observations. An exponential cutoff was applied to the power law continuum with the cutoff energy at 250 keV, chosen to be to match that observed in the average OSSE spectrum of three radio quiet type 2 Seyfert galaxies (NGC 4507, NGC 7582, and MCG–5–23–16; Zdziarski et al. 1995). It can be seen that this is a reasonable description of the OSSE spectrum (Fig. 9, solid line).

A reflection model was applied to the *ASCA*–OSSE data with parameters taken from the average *Ginga*–OSSE spectrum of three type 2 Seyfert galaxies (Zdziarski et al. 1995). The relative normalization of the reflection continuum (\mathfrak{R}) was fixed at 1.3 times the normalization of the power law continuum, and the exponential cutoff for the power law continuum fixed at $E_c = 250$ keV. The other model parameters were taken from Table 2a. It can be seen from Fig. 9 that a reflection model (dotted line) is not a good representation of the OSSE data. The final model applied to the observations is the thermal Comptonization model of Sunyaev & Titarchuk (1980). The parameters are a plasma temperature of $kT = 30$ and optical depth of $\tau = 5.1$ taken from the model found to be a good description of the average OSSE spectrum of 15 Seyfert galaxies (Johnson et al. 1994) and this model shown in Fig. 9 as the dashed continuum. There are very few counts above ~ 1 MeV and with only 6 data points for the OSSE observations the parameters for the models cannot be usefully constrained. However this model appears to have difficulty in reproducing the observed spectrum above 200 keV.

3.7. Spectral Variability

It is immediately obvious on examination of the model parameters in Tables 2a and 2b, and the corresponding χ^2 confidence contours shown in Figs. 4 & 7 that there has been a significant change in the absorbed power law continuum flux in both NGC 4388 and ESO 103–G35, falling by a factor of 2 in the former case and rising by about the same factor in the latter. This can also be seen in Figure 10 where we show the effect of applying the 1993 model of the spectrum of NGC 4388 to the 1995 data and the 1994 model of the spectrum of ESO 103–G35 to the 1996 data. The residuals from these plots clearly show continuum variability in both objects and emission line variability between the observations of NGC 4388. The confidence contours shown in Fig. 7 indicate a possible change in the equivalent width of the Fe K α emission line between the observations of ESO 103–G35. It can also be seen that, although the ratio of the normalizations of the unabsorbed (A_2) to absorbed (A_1) power law continua in the spectra of ESO 103–G35 is $\lesssim 1\%$, it changes between the 1994 and 1996 observations (see Table 2b). This variability is significant at the 90% level (Fig. 7c).

To investigate the significance of these changes further we applied the same models as those described in §3.1 and §3.2 and froze the model parameters that did not appear to change significantly between the observations. These were the power law photon index (Γ), the emission line width (σ), both of the absorbing columns (N_H (1) and N_H (2)) and for NGC 4388, the parameters of the Raymond-Smith component. The fixed parameters were chosen to be the average value from the observations, weighted by the relative error of each measurement. The results are given in Tables 2a,b and the confidence contours for these model fits are shown in Figure 11 where for clarity we only show the confidence limits for 4 IP at the 68% and 99% levels.

What the confidence contours show is very interesting. The probability that the flux

level of the absorbed power law component remained constant between the observations of both NGC 4388 and ESO 103–G35 can be rejected at $\gg 99\%$ (Fig. 11b,e). However we can see that the equivalent width of the Fe $K\alpha$ emission line had remained \sim constant between the two observations of NGC 4388 (Fig. 11a), implying that the emission line flux had fallen by the same level as the underlying continuum. This can be seen in Fig. 11b as a significant (99% confidence) decrease in Fe $K\alpha$ line flux. This is not the case for the observations of ESO 103–G35, there has been a marginally significant (90%) drop in the equivalent width of the line between 1994 and 1996 (Fig. 11d). This can be accounted for by the line flux remaining constant while the underlying continuum rose (Fig. 11e). These effects can also be seen in Fig. 10. Examination of the confidence contours in Fig. 11c,f shows that there has been no significant change in the flux level of the unabsorbed power law continuum (A_2) in the observations of NGC 4388 and ESO 103–G35. Note that this is also true of the flux held in the thermal emission in the spectrum of NGC 4388 if the parameters for this component remain free.

3.8. The simultaneous 1993 *ROSAT* and *ASCA* observation of NGC 4388

Although the *ROSAT* PSPC has a low spectral resolution it may be able to distinguish between thermal and non-thermal models as well as giving an indication of the presence of absorption edges due to a warm absorber (Halpern 1984). The 1993 PSPC spectrum of NGC 4388 was investigated by Rush & Malkan (1996) and it was found that the absorbing column was significantly higher than the Galactic value and that an emission feature may also be present at 0.6 keV. The soft X-ray flux observed by the PSPC in the 1993 observation is somewhat less than that observed during the HRI observation in 1991 but is consistent with the flux measured during the 1993 and 1995 *ASCA* observations.

The serendipitous observations of NGC 4388 in 1993 by *ROSAT* and *ASCA* allowed

for a modeling of the X-ray spectrum from 0.1 to 10 keV. It was found that the model from Table 2a (RS+2PL) could not account for the emission seen by the PSPC below $E < 0.4$ keV ($\chi^2/dof = 363.9/350$). A second, cooler, thermal component with $kT = 0.09 \pm 0.09$ keV was added to the model with an absorbing column found to be at the lower limit set by the measured Galactic column ($N_{\text{H}}^{\text{Gal}} = 2.54 \times 10^{20}$; Murphy et al. 1996). This significantly improved the model fit ($\Delta\chi^2/\Delta dof = 27.7/4$, $0.01 > P_{\text{F-Test}} > 0.001$), the parameters for the remaining components were found to be consistent with those in Table 2a. This is discussed in §4.3.

4. Discussion

The defining characteristic of the X-ray spectra of type 2 Seyfert galaxies is the absorption of a power law continuum by columns of cold gas with $N_{\text{H}} \sim 10^{22}$ to 10^{23} cm^{-2} (Smith & Done 1996; Turner et al. 1997a). Two locations for the absorbing material are generally considered: a torus of optically thick cold gas surrounding the active nucleus and the interstellar medium (ISM) of the host galaxy. The latter may be a reasonable possibility for NGC 4388 and ESO 103–G35 as both AGN lie in highly inclined spiral galaxies. The observed narrow line Balmer decrements are likely to arise in the host galaxy ISM rather than in a unified model torus as the narrow line region is usually thought of as being more spatially extended than the torus. However, the large columns indicated by the X-ray observations of NGC 4388 and ESO 103–G35 are not consistent with the expected neutral hydrogen column of 2 and $8 \times 10^{21} \text{ cm}^{-2}$ (respectively) indicated by the observed optical extinction ($A_{\text{V}} = 0.97$ and 3.72). The existence of an H_2O megamaser with a luminosity of $L_{\text{maser}} = 360L_{\odot}$ in ESO 103–G35 (Braatz et al. 1996) also provides a strong case for the presence of large amounts of cold molecular gas close to the active nucleus. These megamasers have been identified as residing in the molecular torus surrounding the central

engine of a number of AGN and can be used to determine the physical and geometrical properties of the tori (Taniguchi & Murayama 1998 and references therein).

EXOSAT observations of ESO 103–G35 during 1985 appeared to indicate a decline in the absorbing column density over a period of ~ 100 days, and this was interpreted in terms of motion of BLR clouds across the line of sight (Warwick et al. 1988). There is no evidence for variability in the absorbing column from the *ASCA* observations of ESO 103–G35 alone and the column is within the error of that measured during the 1988 and 1991 *Ginga* observations ($1.76^{+0.41}_{-0.31} \times 10^{23} \text{ cm}^{-2}$, Warwick et al. 1993; $2.2 \pm 0.3 \times 10^{23} \text{ cm}^{-2}$, Smith & Done 1996). Examination of the *ROSAT* All-Sky Survey Bright Source Catalog shows a bright soft X-ray source (1RXS J184538.1–645144; $1.07 \pm 0.09 \text{ counts s}^{-1}$) that is $54'$ from the position of ESO 103–G35 and identified with CPD–64 3950, a M0 $m_B = 10.4$ star. This star may be the source of a soft X-ray flare event that occurred during the 1988 *Ginga* LAC observation ($1^\circ \times 2^\circ$ field of view) which is clearly seen in the *Ginga* spectrum as a soft excess above the absorbed power law continuum (Warwick et al. 1993, see Fig. 9). It is unlikely that this source affected the 1995 *EXOSAT* ME observations however as the ME detector had a $45'$ FWHM field of view.

The absorbing material may not have been in a neutral state during the 1996 *ASCA* observation of ESO 103–G35 and the measured ionized absorption edge is in agreement with the edge measured from 1988 *Ginga* observation of $E = 7.68^{+0.12}_{-0.32} \text{ keV}$ (Warwick et al. 1993). An ionized absorption model appears to be a reasonable description of the 1991 *Ginga* spectrum of ESO 103–G35 with a similar flux level to that observed in the 1996 *ASCA* observation. This *Ginga* observation was fitted by a model with $\Gamma = 1.84^{+0.08}_{-0.11}$, $N_H = (3.55^{+0.72}_{-0.56}) \times 10^{23} \text{ cm}^{-2}$, $\xi = 25^{+37}_{-16}$, and $\text{EW Fe K}\alpha = 220^{+100}_{-110} \text{ eV}$ (Smith & Done 1996), all consistent with the ionized absorber model of the 1996 *ASCA* observation presented here (§3.2). A comparison between the 1988 *Ginga* spectrum of ESO 103–G35 and the 1994

and 1996 *ASCA* spectra is presented in Figure 9 along with the model fit to the *Ginga* observation (Warwick et al. 1993). It can be seen that the flux level of the 1996 *ASCA* observation is also consistent with the 1988 *Ginga* observation but that the continuum flux during the 1994 *ASCA* observation was lower than that observed in the *Ginga* observations in 1988 and 1991.

4.1. Fe $K\alpha$ emission line variability

A clue to the location of the absorbing material can come from studying the behavior of the Fe $K\alpha$ emission line compared with changes in continuum flux. No variation in the equivalent width of this line is observed in the spectra of NGC 4388 and this implies that the line flux declined with the continuum. Similar behavior was seen between the *ASCA* observations of the type 2 Seyfert galaxy NGC 7172 (separated by a year) where the equivalent width of the Fe $K\alpha$ line remained the same while the continuum flux declined by a factor of 3 – 4 (Guainazzi et al. 1998). This implies that the line emitting region is within a few light years of the continuum source in these objects. The *Ginga* observations of ESO 103–G35 have indicated an Fe $K\alpha$ emission line with an equivalent width of ~ 250 eV (Warwick et al. 1993; Smith & Done 1996) similar to that observed in the 1996 *ASCA* observation. However the equivalent width of the emission line during the 1994 *ASCA* observation appears larger than during these observations, and this becomes a significant difference when the fixed parameter model is used (Table 2a, Fig. 11d) indicating that the line flux remained \sim constant between the two *ASCA* observations (Fig. 11e). This behavior may be similar to that observed in the intermediate type Seyfert galaxy NGC 2992 and the type 2 Seyfert galaxy Mkn 3 (Weaver et al. 1996; Griffiths et al. 1998), although in an opposite sense with the line flux increasing at a slower rate than the continuum for ESO 103–G35. The measured column densities in the line of sight material towards NGC

4388 and ESO 103–G35 could yield an emission line with an equivalent width of ~ 150 eV for a model where absorption is from a uniform shell of material entirely covering the continuum source (Leahy & Creighton 1993; Awaki et al. 1991). The equivalent width of the Fe $K\alpha$ emission line for the ionized absorption model of the 1996 observation of ESO 103–G35 is 225 eV and this can be accounted for by fluorescence in the line of sight material to within the accuracy of the measurement of the column density. However the large equivalent widths measured in the 1994 observation of ESO 103–G35 and the observations of NGC 4388 imply a source of line photons other than from the line of sight absorbing material and there are a number of possibilities available to explain this disagreement.

- The assumptions of the uniform shell model are incorrect. For instance the column density along our line of sight may be lower than the average, or the X-ray emission may be beamed (e.g. Awaki et al. 1991). The beaming factor would only have to be a modest factor of ~ 3 to give the correct line strengths but this would not account for the change in the equivalent width of the line seen between the *ASCA* observations of ESO 103–G35 unless the beaming parameters had also varied.
- If the absorbing material had the toroidal configuration favored by many unified models of AGN then the excess line photons may be produced from a scattered or reflected component, perhaps from the inner edge of the torus or material out of the plane of viewing (case b in Awaki et al. 1991). This type of model favors a viewing angle close to the opening angle of the torus for ESO 103–G35 as the expected strength of the scattered flux observed in the soft X-ray region is $\sim 1/1000$ that of the primary flux, and this is of the same order of magnitude as the measured value of A_2/A_1 (Table 2b). The higher relative strength of the ‘unabsorbed’ continuum in NGC 4388 (Table 2a) would thus imply a more edge-on viewing angle of the torus as a greater proportion of the primary radiation would be

obscured. Such a reflected or scattered continuum may not have had time to respond to the observed changes in the power law continuum flux, and this is supported by the lack of a significant variation in the observed fluxes of this component in NGC 4388 or ESO 103–G35 (Fig. 11c,f). These observations then imply that the inner edge of the torus would lie ~ 1.5 or 2 light years from the continuum source in ESO 103–G35 and NGC 4388 respectively.

- An abundance of iron at a factor of > 10 times Solar in the absorbing material observed in the *ASCA* spectra of ESO 103–G35 and NGC 4388 would be required to account for the high equivalent widths (George & Fabian 1991) and this would also cause the Fe K edge to be much stronger than is observed (see §3.3).
- The high column density material in the leaky-absorber model for the type 2 Seyfert galaxy IRAS 04575–7537 was interpreted as arising in BLR clouds (Vignali et al. 1998). However in that case the covering fraction was significantly lower (36%) than seen in NGC 4388 (§3.5 and Table 3) and much closer to the 10% value normally associated with the BLR in AGN. What we may be seeing in NGC 4388 is the presence of clumping in a unified model type torus, although we can not rule out the ISM of the host galaxy of NGC 4388 as the location of the absorbing material because the stellar disk of NGC 4388 has a high inclination to the line of sight. The optical depth required to account for the strength of the Fe K α emission line in NGC 4388 ($\tau_{\text{FeK}} \sim 1$) is also at the upper limit of the 99% error margin on the measured value as can be seen in Fig. 8. Similarly we can interpret the presence of a less absorbed power law continuum in NGC 4388 as evidence that the covering fraction of the lower column density absorber is less than unity (90 – 95%), although this is difficult to reconcile with a model of absorption in the ISM. The leaky-absorber model applied to the *ASCA* spectra of ESO 103–G35 causes the power law continuum to become rather steep ($\Gamma \gtrsim 2.2$) and, although the presence of a larger absorbing column will reconcile the high equivalent width of the Fe K α emission line seen in

the 1994 spectrum, it predicts an equivalent width higher than is seen in the 1996 spectrum. This model also does not seem to agree with the variability behavior of the Fe K α emission line and Fe K edge. The optical depth of the Fe K edge is seen to increase between the observations and this implies that the strength of the Fe K α emission line should have increased but the opposite behavior is seen (Figs. 8 and 11).

4.2. No reflection continuum in NGC 4388 or ESO 103–G35

In many type 1 Seyfert galaxies strong Fe K α emission lines are observed, some with complex profiles and large equivalent widths (Nandra et al. 1997). The interpretation is that of fluorescence from an accretion disk, however the material in this case is close to (or coincident with) the source of the continuum photons and so no lag in line response is expected (e.g. MCG –5–23-16, Weaver, Krolik, & Pier 1998; Nandra et al. 1997). Turner et al. (1998) found evidence for broad Fe K α line emission in up to a third of their sample of narrow-line AGN which they modeled as emission from an accretion disk viewed ‘pole-on’ (i.e. similar to emission seen in type 1 AGN). No evidence for a significant broad line is found here for NGC 4388 or ESO 103–G35. The identification of a broad Fe K α line in the 1994 *ASCA* spectrum of ESO 103–G35 by Turner et al. (1998) at the 90% confidence level, with $\sigma = 310$ eV and $EW = 505$ eV, differs from the results presented here of a single *unresolved* narrow emission line (see Table 2b and Fig. 7). This could be due to differences in the continuum model, Turner et al. (1998) finding a flatter power law and a lower column density although the measurements presented here agree to within their 90% confidence limits. Four of the sample of narrow line Seyfert galaxies studied by Turner et al. (1998) have also been successfully modeled by Weaver & Reynolds (1998) with a combination of a broad component from an accretion disk viewed at an inclination angle of $\sim 48^\circ$ and a narrow unresolved component. This illustrates the difficulty of identifying broad emission

features on heavily absorbed power law spectra with low signal-to-noise data.

In type 2 Seyfert galaxies where the power law continuum slope is very flat and the observed equivalent widths of the Fe $K\alpha$ line are extremely large, a reflection continuum is thought to be the dominant component in the hard X-ray continuum. This is the case for NGC 1068, where *ASCA* observations have revealed a complex blend of neutral and ionized Fe $K\alpha$ emission lines with equivalent widths $\gtrsim 1$ keV (Ueno et al. 1994) and in the Circinus galaxy, NGC 6552, and NGC 7674, where equivalent widths larger than 1 keV are also seen (Matt et al. 1996; Reynolds et al. 1994; Malaguti et al. 1998 respectively). Nevertheless, the presence of a reflection component will increase the observed strength of the Fe $K\alpha$ emission lines as well as cause a flattening of the power law continuum, although a flat hard X-ray spectral slope does not necessarily require a dominant reflection component, as is the case for NGC 5252 (Cappi et al. 1996). In this type 2 Seyfert galaxy the equivalent width of the Fe $K\alpha$ emission line is very low (~ 100 eV), and although the combination of a partially covered power law continuum and a reflection component can account for the flat spectrum ($\Gamma = 1.45 \pm 0.23$), the model predicts an emission line of equivalent width ~ 400 eV, much larger than is observed. This situation may also be relevant for NGC 7582 where a very flat hard X-ray power law continuum is identified ($\Gamma = 0.7^{+0.3}_{-0.4}$) absorbed by a column $N_{\text{H}} = 5^{+2}_{-1} \times 10^{22} \text{ cm}^{-2}$ (Schachter et al. 1998). However only an upper limit of a few 100 eV could be placed on the equivalent width of an Fe $K\alpha$ line and so no reflection continuum is likely to be present. The intermediate strength Fe $K\alpha$ emission line observed in NGC 4388 may then indicate that a reflection component is present but does not dominate the hard X-ray continuum.

The combined *ASCA* and OSSE spectrum of NGC 4388 is also similar to that of NGC 4507 and NGC 7172 where OSSE observations combined with *Ginga* and *ASCA* observations (respectively) of these AGN do not require a reflection component and can

be fitted with exponentially cut off power law continua (Bassani et al. 1995; Ryde et al. 1997). Although both of these type 2 Seyfert galaxies have a heavily absorbed flat power law continuum, the Fe K α emission line equivalent widths of ~ 300 and 100 eV respectively are consistent with fluorescence through the line of sight absorbing columns (Comastri et al. 1998; Guainazzi et al. 1998) and so no reflection component is required. The *ASCA* observations of NGC 7172 separated by one year also showed that while the continuum flux declined by a factor of 3–4 the equivalent width of the Fe K α line remained the same (Guainazzi et al. 1998). This is similar to the behavior seen in the *ASCA* observations of NGC 4388 presented here.

For the *Ginga* observations of ESO 103–G35, Smith & Done (1996) find that a model with a reflection component is as good a fit as the ionized absorption model. The reflection model required that $\Gamma = 2.19^{+0.09}_{-0.15}$, $N_{\text{H}} = (2.42^{+0.26}_{-0.23}) \times 10^{23} \text{ cm}^{-2}$, $\Re = 2.00^{+0.48}_{-0.95}$, with an Fe K α equivalent width of < 175 eV. When a reflection model was applied to the 1996 *ASCA* spectrum a similar result was obtained with no improvement over the model presented in Table 2b ($\chi^2/dof = 532.6/524$) however, the reflection model parameters could not be constrained due to the limit of the bandpass of the *ASCA* instruments. The lower equivalent width of the Fe K α emission line seen during 1996 *ASCA* observation of ESO 103–G35 does not require a reflection component and can be accounted for by line of sight fluorescence in material with the measured column density alone.

We conclude that the *ASCA* observations of both NGC 4388 and ESO 103–G35 do not require a reflection component.

NOTE ADDED IN PROOF. A stronger constraint is found from the October 1996 and 1997 BeppoSAX observations of ESO 103–G35 where a reflection component is indicated in a spectrum that extends up to ~ 200 keV (Wilkes et al. 1999, in preparation).

4.3. Soft X-ray emission

Significant low energy emission lines identified with elements lighter than iron are also present in the spectra of reflection dominated Seyfert galaxies as predicted in models of reflection from cold material (Reynolds et al. 1994; Netzer et al. 1998). If a reflection component were strong in the X-ray spectra of either NGC 4388 or ESO 103–G35 then low energy emission features may also be present. Determination of such features in the spectrum of NGC 4388 is complicated by the extended thermal emission seen in the *ROSAT* HRI observation (Matt et al. 1994). The model of the combined *ROSAT* PSPC and *ASCA* spectrum of NGC 4388 gives a soft X-ray (0.2 – 4.0 keV) flux of $f_X = 7.8 \times 10^{-13}$ ergs cm $^{-2}$ s $^{-1}$ and this is consistent with the total fluxes seen in the 1991 HRI observation of $(6.75 \pm 0.72) \times 10^{-13}$ ergs cm $^{-2}$ s $^{-1}$ and in the 1978 *Einstein* IPC observation of 6.6×10^{-13} ergs cm $^{-2}$ s $^{-1}$, (Matt et al. 1994; Fabbiano, et al. 1992). The radial profile of the soft X-ray emission, observed by the HRI to extend out to ~ 4.5 kpc, suggests that $\sim 20\%$ of this flux is from a nuclear component within a radius 1.5 kpc. The expected 2 – 4 keV luminosity from the host spiral galaxy of the AGN in NGC 4388 is $L_X = 6.17 \times 10^{39}$ erg s $^{-1}$, scaling from the B-band luminosity (Fabbiano et al. 1992). Combined with the observed kiloparsec-scale emission (Colbert et al. 1998) this can fully account for the thermal emission observed in the *ASCA* spectra. Netzer et al. (1998) have modeled emission features below 3 keV in the 1993 *ASCA* spectrum of NGC 4388 as due to a scattering process, however these features may be due to the thermal component. The addition of Gaussian emission lines to the spectrum between 1.5 and 3.0 keV does not improve the chi-square residuals significantly and a scattered continuum cannot explain the nature of the bulk of the soft X-ray emission seen in NGC 4388. The temperature of the thermal components measured in the combined *ROSAT* – *ASCA* observation are too cool to be identified with a typical soft X-ray spectrum from a starburst disk (Ptak 1997) or ram pressure stripped hot gas (e.g. Irwin & Sarazin 1996; Hwang & Sarazin 1996). The

combined emission from a collection of LMXB’s in the bulge of NGC 4388 may prove to be the most straightforward explanation of the nature of the extended soft X-ray emission (Irwin & Sarazin 1998). The high spatial resolution of a *Chandra* observation should prove useful in distinguishing between the various possibilities.

The *ROSAT* PSPC image of ESO 103–G35 shows only a weak unresolved nuclear soft X-ray source with a 0.5 – 2.0 keV flux of 5×10^{-14} ergs cm $^{-2}$ s $^{-1}$. This is consistent with the flux observed during the 1994 *ASCA* observation and this poses a problem. Two nearby soft X-ray sources (see §2.2) should have contaminated the GIS observations with a combined soft X-ray flux at least 4 times larger than that observed from ESO 103–G35 during the PSPC observation. Although the soft X-ray flux appears to have risen slightly (9×10^{-14} ergs cm $^{-2}$ s $^{-1}$) in the 1996 *ASCA* observation this is still too low and this may either indicate a problem with the cross calibration between the *ROSAT* and *ASCA* instruments or variability of the contaminating sources. The increase in soft X-ray flux between the 1994 and 1996 observations may indicate an emergence of scattered or leaked nuclear flux that adds to the soft X-ray emission from the host galaxy and this could account for the rise in A_2/A_1 when the absorbed power law continuum also rose by a factor of 2 between the observations. There is also an emission feature near 0.9 keV in the spectrum of ESO 103–G35 (Fig. 5) that may be similar to that seen in the soft X-ray spectra of NGC 4507 and Mkn 3 (Comastri et al. 1998; Griffiths et al. 1998). This was interpreted as Ne IX K α recombination from a photoionized plasma in the case of NGC 4507 and this may also be the case for ESO 103–G35. Again, the capabilities of *Chandra* should resolve these possibilities.

5. Summary and conclusions

ASCA observations of two intermediate type Seyfert galaxies NGC 4388 and ESO 103–G35 have been investigated and combined with *ROSAT* PSPC and *CGRO* OSSE observations.

The *ASCA* spectrum of NGC 4388 can be described by a heavily absorbed flat power law continuum ($\Gamma = 1.4$, $N_{\text{H}} = 3.3 \times 10^{23} \text{ cm}^{-2}$) with a strong Fe $K\alpha$ emission line ($EW = 720 \text{ eV}$) and soft X-ray thermal emission ($kT = 0.17 \text{ keV}$). The data also require the presence of a second, less absorbed, power law continuum at $\sim 5\%$ the flux level of the absorbed continuum. The equivalent width of the Fe $K\alpha$ emission line requires a larger column of absorbing material than is measured and the power law continuum is flatter than the canonical Seyfert galaxy spectral slope. Both of these properties are characteristic of reflection dominated type 2 Seyfert galaxies. However the model fit is not improved by the inclusion of a Compton reflection component, and there is also a concern that the modeling of the contemporary 1993 *ASCA* and OSSE observations do not appear to require a reflection continuum and can be fitted with a flat power law with an exponential cut off at high energies. NGC 4388 may be a case where there is a relatively small amount of reflection that manifests itself in a stronger than expected Fe $K\alpha$ emission line. NGC 4388 would then lie somewhere between NGC 5252 and the Compton-thick type 2 Seyfert galaxies in terms of the relative strength of the reflection component to the direct absorbed continuum.

A leaky-absorber model is able to reconcile the strength of the Fe $K\alpha$ line and the ‘low’ measured absorbing column. In this model there are two distinct absorbing media, the first has a column of $N_{\text{H}} = 5 - 10 \times 10^{23} \text{ cm}^{-2}$ and a covering fraction of $\sim 70\%$ and the second a lower column of $N_{\text{H}} = 3 \times 10^{23} \text{ cm}^{-2}$. The strength of the Fe $K\alpha$ line is then fully accounted for; however the observed optical depth at the Fe K edge is somewhat

smaller than expected from material with such a large column and the model is unable to improve statistically on the absorbed flat power law continuum model. The high column density gas component in the leaky-absorber model may reside in a hidden BLR of NGC 4388 (although the covering fraction is higher than normally associated with BLR clouds) a molecular torus surrounding the active nucleus, or the host galaxy ISM. The *ASCA* observations are not sufficient to distinguish between these possibilities. The nature of the soft X-ray thermal emission seen in the *ASCA* observations of NGC 4388 is consistent with an identification with the extended emission seen in a *ROSAT* HRI observation. However, higher spatial and spectral resolution will be required to investigate the true nature of the extended emission.

The spectrum of the intermediate type Seyfert galaxy ESO 103–G35 can be well characterized by a heavily absorbed power law continuum of slope $\Gamma = 1.8$ and $N_{\text{H}} = 2.0 \times 10^{23} \text{ cm}^{-2}$. This continuum was observed to increase in flux by a factor of 2 between the *ASCA* observations separated by 18 months. However the equivalent width of the Fe K α emission line was seen to decrease between these observations implying that the line flux remained \sim constant. The optical depth of the Fe K edge is also observed to increase between the *ASCA* observations and the edge energy in the later observation indicates absorption from partially ionized iron. This matches the results of the 1998 and 1991 *Ginga* observations (Warwick et al. 1993; Smith & Done 1996). These, and the *EXOSAT* observations taken between 1983 and 1985 (Turner & Pounds 1989), also showed ESO 103–G35 to have a similar 2 – 10 keV luminosity to that seen in the 1996 *ASCA* observation.

A Compton reflection component can be included in the continuum model but is not required on statistical grounds or needed to steepen the power law continuum to comply with the canonical Seyfert galaxy spectral slope. It is also not required to reconcile the Fe

$K\alpha$ emission line strength in the 1996 observation as this is consistent with fluorescence from partially ionized material with the measured column density. However the strength of the line in the 1994 *ASCA* observation indicates that an additional source of line photons is needed but a dual absorber model is inconsistent with the observed optical depth of the Fe K edge. One (highly speculative) possibility is that the Fe $K\alpha$ emission line is responding to a higher X-ray flux level previous to the 1994 *ASCA* observation.

In terms of a unified model of Seyfert galaxies these intermediate type AGN exhibit an X-ray spectrum very similar to that seen in many type 2 Seyfert galaxies but are certainly not reflection dominated and do not require the addition of a reflection continuum to explain the properties observed in the *ROSAT*, *ASCA* and OSSE observations presented here.

This paper is contribution No. 677 of the Columbia Astrophysics Laboratory. KML gratefully acknowledges support through NAG5-3307 (*ASCA*). This research has made use of the NASA/IPAC Extragalactic Database (NED) which is operated by the Jet Propulsion Laboratory, California Institute of Technology, under contract with the National Aeronautics and Space Administration. This research has also made use of data obtained from the High Energy Astrophysics Science Archive Research Center (HEASARC), provided by NASA’s Goddard Space Flight Center.

REFERENCES

- Arnaud, K.A., 1996, “Astronomical Data Analysis Software and Systems. V”, eds. G. Jacoby, & J. Barnes, ASP Conf. Series, 101, p17
- Awaki, H., Koyama, K., Inoue, H., & Halpern, J.P. 1991, PASJ, 43, 195
- Awaki, H., et al. 1994, PASJ, 46, L65
- Bassani, L., Malaguti, G., Jourdain, E., Roques, J.P., & Johnson, W.N. 1995, ApJ, 444, L73
- Bevington, P.R., & Robinson, D.K. 1992, “Data reduction and error analysis for the physical sciences”, 2nd ed. (New York:McGraw-Hill)
- Blanco, P.R., Ward, M.J., & Wright, G.S. 1990, MNRAS, 242, L4
- Braatz, J.A., Wilson, A.S., & Henkel, C. 1996, ApJS, 106, 51
- Cappi, M., Mihara, T., Matsuoka, M., Brinkmann, W., Prieto, M.A., & Palumbo, G.G. 1996, ApJ, 456, 141
- Colbert, E.J.M., Baum, S.A., O’Dea C.P., & Veilleu, S. 1998, ApJ, 496, 786
- Comastri, A., Vignali, C., Cappi, M., Matt, G., Audano, R., Awaki, H., & Ueno, S. 1998, MNRAS, 295, 443
- Day, C., et al. 1995, “The *ASCA* Data Reduction Guide”, Version 2.0, ASCA GOF, LHEA,
- Dotani, T., Yamashita, A., Rasmussen, A. and the SIS team 1995, “Effects of radiation damage on SIS performance” *ASCA* Newsletter number 3, p25.
(http://heasarc.gsfc.nasa.gov/docs/ASCA/newsletters/rad_dam_sis3.html)
- Dotani, T., Mitsuda, K., Ezuka, H., Hayashida, K., Torii, K., Miura, N., Otani, C., Crew, G., Rasmussen, A., & Gendreau, K. 1996, “SIS Calibration and Software: Recent Developments” *ASCA* Newsletter 4, p3.
(http://heasarc.gsfc.nasa.gov/docs/ASCA/newsletters/sis_calibration4.html)

- Fabbiano, G., Kim D.-W., & Trinchieri, G. 1992, *ApJS*, 80, 531
- Filippenko, A.V., & Sargent, W.L. 1985, *ApJS*, 57, 503
- Filippenko, A.V. 1996, in “The Physics of LINERs in view of recent observations”, eds M. Eracleous, A. Koratkar, C. Leitherer, & L. Ho, ASP conference series, 103, p17
- George, I.M., & Fabian, A.C. 1991, *MNRAS*, 249, 352
- Goodrich, R.W., Veilleux, S., & Hill, G.J. 1994, *ApJ*, 422, 521
- Griffiths, R.G., Warwick, R.S., Georgantopoulos, I., Done, C., & Smith, D.A. 1998, *MNRAS*, 298, 1159
- Guainazzi, M., Matt, G., Antonelli, L.A., Fiore, F., Piro, L., & Ueno, S. 1998, *MNRAS*, 298, 824
- Halpern, J.P. 1984, *ApJ*, 281, 90
- Hanson, C.G., Skinner, G.K., Eyles, C.J., & Willmore, A.P. 1990, *MNRAS*, 242, 262
- Heckman, T.M. 1980, *A&A*, 87, 152
- Helou, G., Salpeter, E.E., Giovanardi, C., & Krumm, N. 1981, *ApJS*, 46, 267
- Hwang, Z., & Sarazin, C.L. 1996, *ApJ*, 461, 622
- Irwin, J.A., & Sarazin, C.L. 1996, *ApJ*, 471, 683
- Irwin, J.A., & Sarazin, C.L. 1998, *ApJ*, 494, L33
- Iwasawa, K., Fabian, A. C., Ueno, S., Awaki, H., Fukazawa, Y., Matsushita, K., & Makishima, K. 1997, *MNRAS*, 285, 683 (I97)
- Johnson, W.N., Kinzer, R.L., Kurfess, J.D., Strickman, M.S., Purcell, W.R., Grabelsky, D.A., Ulmer, M.P., Hillis, D.A., Jung, G.V., Cameron, R.A. 1993, *ApJS*, 86, 693
- Johnson, W.N., Grove, J.E., Kinzer, R.L., Kroeger, R.A., Kurfess, J.D., Strickman, M.S., McNaron-Brown, K. , Grabelsky, D.A., Purcell, W.R., Ulmer, M.P., & Jung, G.V. 1994, in

- Second Compton Observatory Symp. eds C.E. Fichtel, et al. (New York:AIP), p515
- Kallman, T.R., & McCray, R. 1982, ApJS, 50, 263
- Kay, L.E. 1994, ApJ, 430, 196
- Kirhakos, S.D., & Steiner, J.E. 1990, AJ, 99, 1722
- Kurfess, J.D. 1994, in IAU symp. 159, “Multiwavelength continuum emission of AGN”, eds T.J.-L. Courvoisier and A. Blecha (Kluwer:1994), p39
- Leahy, D.A., & Creighton, J. 1993, MNRAS, 263, 314
- Lightman, A.P., & White, T.R. 1988, ApJ, 335, 57
- Malaguti, G., Palumbo, G.G.C., Cappi, M., Comastri, A., Otani, C., Matsuoka, M., Guainazzi, M., Bassani, L., & Frontera, F. 1998, A&A, 331, 519
- Matt, G., Fabian, A.C., & Ross, R.R. 1993, MNRAS, 262, 179
- Matt, G., Piro, L., Antonelli, L.A., Fink, H.H., Meurs, E.J.A., & Perola, G.C. 1994, A&A, 292, L13
- Matt, G., Brandt, W.N., & Fabian, A.C. 1996, MNRAS, 280, 823
- Matt, G., Fiore, F., Perola, G.C., Piro, L., Fink, H.H., Grandi, P., Matsuoka, M., Oliva, E., & Salvati, M. 1996, MNRAS, 281, L69
- Murphy, E.M., Lockman, F.J., Laor, A., & Elvis, M. 1996, ApJS, 105, 369
- Nandra, K., & Pounds, K.A. 1994, MNRAS, 268, 405
- Nandra, K., George, I.M., Mushotzky, R.F., Turner, T.J., & Yaqoob, T. 1997, ApJ, 477, 602
- Netzer, H. 1996, ApJ, 473, 781
- Netzer, H., Turner, T.J., & George, I.M. 1998, ApJ, 504, 680
- Phillips, M.M., Feldman, F.R., Marshall, F.E., & Wansteker, W. 1979, A&A, 76, L14

- Ptak, A.F. 1997, PhD Thesis, University of Maryland
- Raymond, J.C., & Smith, B.W. 1977, *ApJS*, 35, 419
- Reynolds, C.S., Fabian, A.C., Makishima, K., Fukazawa, Y., & Tamura, T. 1994, *MNRAS*, 268, L55
- Roche, P.F., Aitken, D.K., Smith, C.H., & Ward, M.J. 1991, *MNRAS*, 248, 606
- Ruiz, M., Rieke, G.H., & Schmidt, G.D. 1994, *ApJ*, 423, 608
- Rush, B., & Malkan, M.A. 1996, *ApJ*, 456, 466
- Ryde, F., Poutanen, J., Svensson, R., Larsson, S., & Ueno, S. 1997, *A&A*, 328, 69
- Schachter, J.F., Fiore, F., Elvis, M., Mathur, S., Wilson, A.S., Morse, J.A., Awaki, H., & Iwasawa, K. 1998, *ApJ*, 503, L123
- Shields, J.C., & Filippenko, A.V. 1988, *ApJ*, 332, L55
- Shields, J.C., & Filippenko, A.V. 1996, *A&A*, 311, 393
- Smith, D.A., & Done, C. 1996, *MNRAS*, 280, 355
- Stark, A.A., Gammie, C.F., Wilson, R.W., Bally, J., Linke, R.A., Heiles, C., & Hurwitz, M. 1992, *ApJS*, 79, 77
- Stauffer, J.R. 1982, *ApJ*, 262, 66
- Sunyaev, R.A., & Titarchuk, L.G. 1980, *A&A*, 86, 121
- Takano, S., Awaki, H., Koyama, K., Kunieda, H., & Tawara, Y. 1989, *Nature*, 340, 289
- Takano, S., & Koyama, K. 1991, *PASJ*, 43, 1
- Taniguchi, Y., & Murayama, T. 1998, *ApJ*, 501, L25
- Turner, T.J. 1996, “ROSAT data analysis using xselect and ftools”, OGIP Memo OGIP/94-010 (http://heasarc.gsfc.nasa.gov/docs/rosat/ros_xselect_guide/xselect_ftools.html)
- Turner, T.J., & Pounds, K.A. 1989, *MNRAS*, 240, 883

- Turner, T.J., Done, C., Mushotzky, R., Madejski, G., & Kunieda, H. 1992, *ApJ*, 391, 102
- Turner, T. J., George, I. M., Nandra, K., & Mushotzky, R. F. 1997a, *ApJS*, 113, 23
- Turner, T.J., George, I.M., Nandra, K., & Mushotzky, R.F. 1997b, *ApJ*, 488, 164
- Turner, T.J., George, I.M., Nandra, K., & Mushotzky, R.F. 1998, *ApJ*, 493, 91
- Ueno, S., Mushotzky, R.F., Koyama, K., Iwasawa, K., Awaki, H., & Hayashi, I. 1994, *PASJ*, 46, L71
- Ueno S. 1997, PhD Thesis, Kyoto University, (ISAS research note 619).
- Vignali, C., Comastri, A., Stirpe, G.M., Cappi, M., Palumbo, G., Matsuoka, M., Malaguti, G., & Bassani, L. 1998, *A&A*, 333, 411
- Warwick, R.S., Pounds, K.A., & Turner, T.J. 1988, *MNRAS*, 231, 1145
- Warwick, R.S., Sembay, S., Yaqoob, T., Makishima, K., Ohashi, T., Tashiro, M., & Kohmura, Y. 1993, *MNRAS*, 265, 412
- Weaver, K.A., Yaqoob, T., Holt, S.S., Mushotzky, R.F., Matsuoka, M., & Yamauchi, M. 1994, *ApJ*, 436, L27
- Weaver, K.A., Nousek, J., Yaqoob, T., Mushotzky, R.F., Makino, F., & Otani, C. 1996, *ApJ*, 458, 160
- Weaver, K.A., Krolik, J.H., & Pier, E.A., 1998, *ApJ*, 498, 213
- Weaver, K.A., & Reynolds, C.S. 1998, *ApJ*, 503, L39
- Wroblewski, H., & Torres, C. 1994, *A&A*, 105, 179
- Yaqoob, T. 1998, *ApJ*, 500, 893
- Young, S., Hough, J.H., Efsthathiou, A., Wills, B.J., Bailey, J.A., Ward, M.J., & Axon, D.J. 1996, *MNRAS*, 281, 1206

Zdziarski, A.A., Johnson, W.N., Done, C., Smith, D., & McNaron-Brown, K. 1995, ApJ, 438, L63

Fig. 1 — The 2 – 10 keV light curve for the 1996 *ASCA* observation of ESO 103–G35. The data is background subtracted and summed over a full orbit (5760s). ● — Summed GIS detectors, □ — Summed SIS detectors. The length of the horizontal error bars is a measure of the fraction of GTI within a 5760 second bin.

Fig. 2 — Residuals from an absorbed power law continuum model fit to the 1993 and 1995 *ASCA* spectra of NGC 4388. Only the SIS data are shown for clarity. Residuals near 6.4 keV suggest the presence of an emission line and there is a significant ‘soft excess’.

Fig. 3 — *ASCA* spectra of NGC 4388 in 1993 and 1995. Only the SIS data are shown and have been rebinned for clarity. *Top panels* — The data and model unfolded from the instrumental response. The shaded areas represent the Raymond–Smith thermal plasma emission ($E \lesssim 2$ keV), the absorbed power law continuum emission ($E > 3$ keV), and the darker shaded region marks the Fe $K\alpha$ emission line. The unshaded component is the less absorbed power law continuum. *Bottom panels* — The ratio of the model to the data.

Fig. 4 — Confidence contours for the model parameters of the simultaneous fit to the GIS and SIS *ASCA* spectra of NGC 4388 in 1993 and 1995 (see Table 2a). Contours represent $\Delta\chi^2$ confidence limits (68%, 90%, and 99%) for 4 interesting parameters (IP). *Solid line* – 1993 observation, *dashed line* – 1995 observation. (a) Power law photon index vs. absorbing column (10^{22} cm $^{-2}$). (b) Power law photon index vs. absorbed power law continuum normalization (photons cm $^{-2}$ s $^{-1}$ keV $^{-1}$). (c) Power law photon index vs. ratio of the normalizations of the unabsorbed to absorbed power law continuum (A_2/A_1). (d) Emission line peak energy (keV) vs. emission line width (keV). (e) Emission line peak energy (keV) vs. equivalent width of the line (keV). (f) Temperature of the Raymond-Smith component (keV) vs. second absorbing column (10^{22} cm $^{-2}$), here the contours are $\Delta\chi^2$ for 2 IP.

Fig. 5 — Residuals from an absorbed power law continuum model fit to the 1994, 1995, and 1996 *ASCA* spectra of ESO 103–G35. Only the SIS data are shown for clarity.

Fig. 6 — *ASCA* spectra of ESO 103–G35 in 1994, 1995, and 1996. Only the SIS data are shown and have been rebinned for clarity. *Top panels* — The data and model unfolded from the instrumental response. The shaded area represents the absorbed power law continuum emission, and the darker shaded region marks the Fe K α emission line. *Bottom panels* — The ratio of the model to the data.

Fig. 7 — Confidence contours for the model parameters of the simultaneous fit to the 1994, 1995 and 1996 *ASCA* GIS and SIS spectra of ESO 103–G35 (see Table 2b). *Solid line* – 1994 observation, *dotted line* – 1995 observation, *dashed line* – 1996 observation. (a – e) See caption for Fig. 4. Note that only the 99% confidence contours are shown in panel b for clarity.

Fig. 8 — Confidence contours for the model parameters of the Fe K absorption edge in the *ASCA* spectra of NGC 4388 and ESO 103–G35. Contours are 68%, 90% and 99% confidence limits for 2 IP. *Solid lines* – 1993/94 observations (NGC 4388/ESO 103–G35). *Dashed lines* – 1995/96 observations. The best fitted value for the 1993 observation of NGC 4388 is represented by a smaller cross.

Fig. 9 — *Left* — The X-ray spectrum of NGC 4388 from 0.1 to 10^4 keV. The *ROSAT* PSPC and *ASCA* SIS model (§3.8) is used with an exponential cutoff (solid line) to extend out to the 1993 *CGRO* OSSE observation. The dotted line is a Compton reflection spectrum and the dashed line (lower line) is a thermal Comptonization model. All *ASCA* instruments were modeled simultaneously with the PSPC data, but only the rebinned data from the SIS 0 instrument is shown for clarity. *Right* — The 1988 *Ginga* observation of ESO 103–G35 (diamonds) shown with the 1994 (black square) and 1996 (crosses) *ASCA* SIS 0 observations. The model is that for the *Ginga* observation with an ionized Fe K edge (Warwick et al. 1993). The rise in the *Ginga* spectrum below 3 keV has been attributed to a contaminating soft X-ray source in the field of view of the *Ginga* LAC (Warwick et al.

1993).

Fig. 10 — Hard X-ray variability of NGC 4388 and ESO 103–G35, both GIS and SIS data are shown. *Top* – The residuals from applying the 1993 model (Table 2a) to the 1995 data of NGC 4388. The variability in the strength of the Fe $K\alpha$ emission line near 6.4 keV can clearly be seen. *Bottom* – As above but applying the 1994 model (Table 2b) to the 1996 data of ESO 103–G35.

Fig. 11 — The confidence contours of the fixed parameter model in Tables 2a,b. The contours are the 68% and 99% confidence contours for 4 interesting parameters. *Top panels* — NGC 4388, *solid line* = 1993 spectrum, *dashed line* = 1995 spectrum. *Bottom panels* — ESO 103–G35, *solid line* = 1994 spectrum, *dotted line* = 1995 spectrum, *dashed line* = 1996 spectrum. (a,d) Emission line peak energy (keV) vs. emission line equivalent width (keV). (b,e) Total photons held in the emission line (10^{-4} photons $\text{cm}^{-2} \text{s}^{-1}$) vs. normalization of the absorbed power law continuum (10^{-3} (b) 10^{-2} (e) photons $\text{cm}^{-2} \text{s}^{-1} \text{keV}^{-1}$ at 1 keV). (c,f) Normalization of the unabsorbed power law continuum ($A_2 \times 10^{-4}$ photons $\text{cm}^{-2} \text{s}^{-1} \text{keV}^{-1}$ at 1 keV) vs. normalization of the absorbed power law continuum ($A_1 \times 10^{-3}$ photons $\text{cm}^{-2} \text{s}^{-1} \text{keV}^{-1}$ at 1 keV).

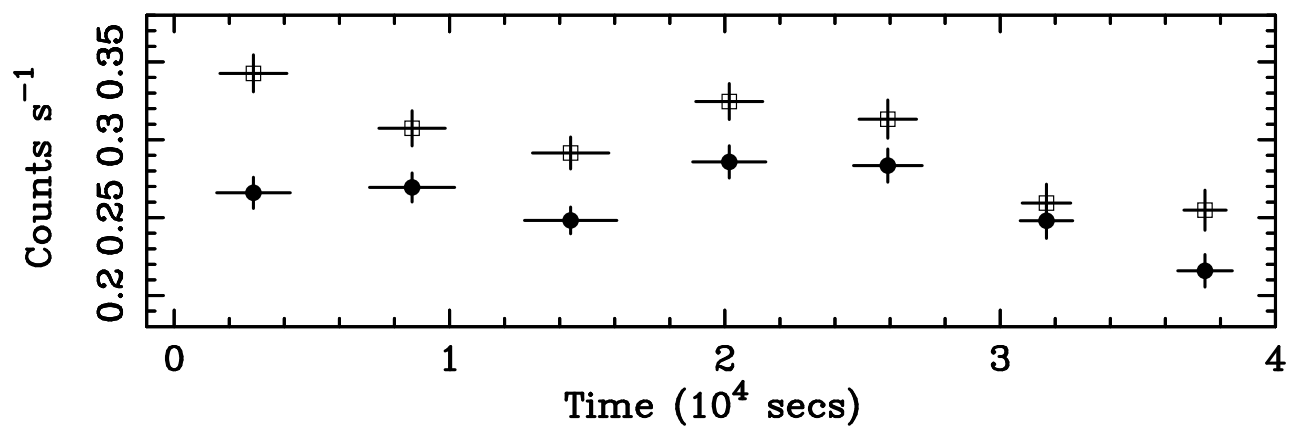


Fig. 1.— The 2 – 10 keV light curve for the 1996 *ASCA* observation of ESO 103–G35. The data is background subtracted and summed over a full orbit (5760s). • — Summed GIS detectors, □ — Summed SIS detectors. The length of the horizontal error bars is a measure of the fraction of GTI within a 5760 second bin.

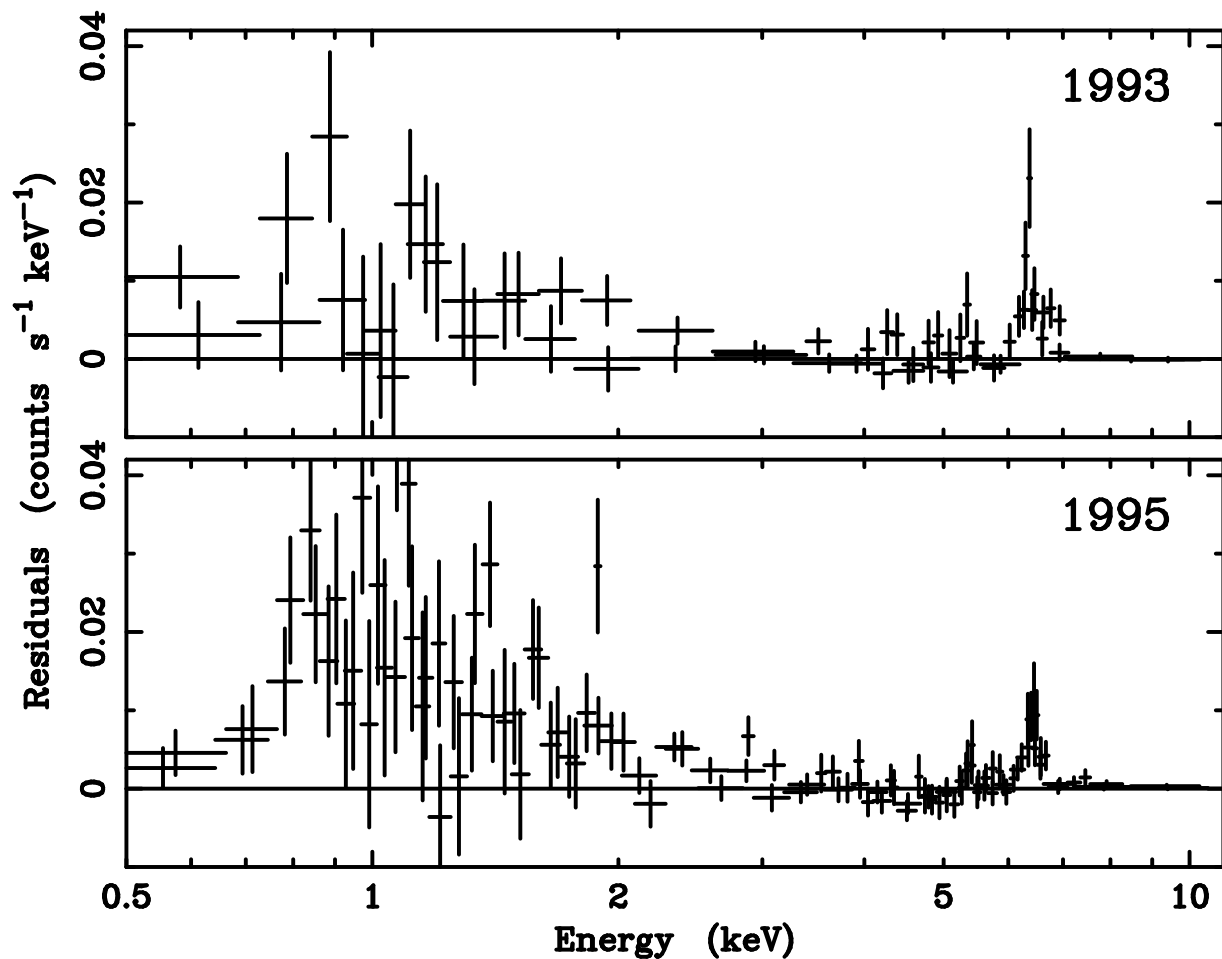


Fig. 2.— Residuals from an absorbed power law continuum model fit to the 1993 and 1995 *ASCA* spectra of NGC 4388. Only the SIS data are shown for clarity. Residuals near 6.4 keV suggest the presence of an emission line and there is a significant ‘soft excess’.

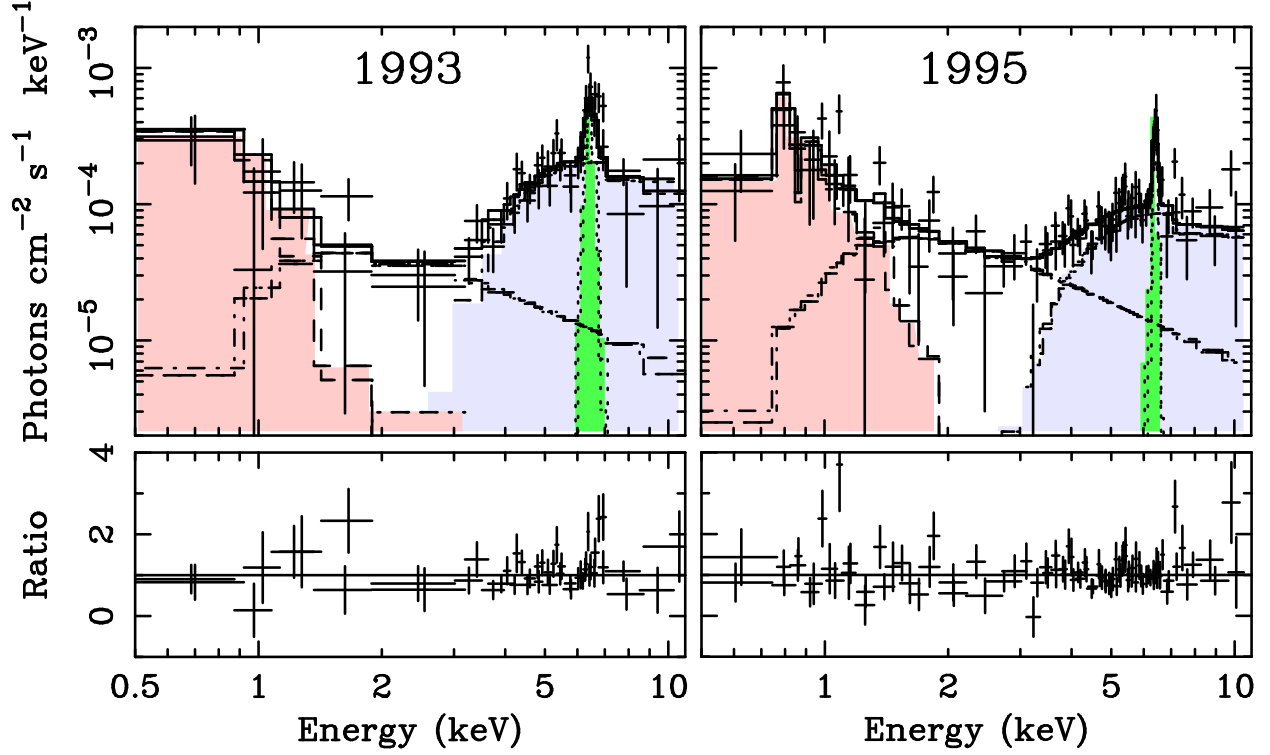


Fig. 3.— *ASCA* spectra of NGC 4388 in 1993 and 1995. Only the SIS data are shown and have been rebinned for clarity. *Top panels* — The data and model unfolded from the instrumental response. The shaded areas represent the Raymond-Smith thermal plasma emission ($E \lesssim 2$ keV), the absorbed power law continuum emission ($E > 3$ keV), and the darker shaded region marks the Fe $K\alpha$ emission line. The unshaded component is the less absorbed power law continuum. *Bottom panels* — The ratio of the model to the data.

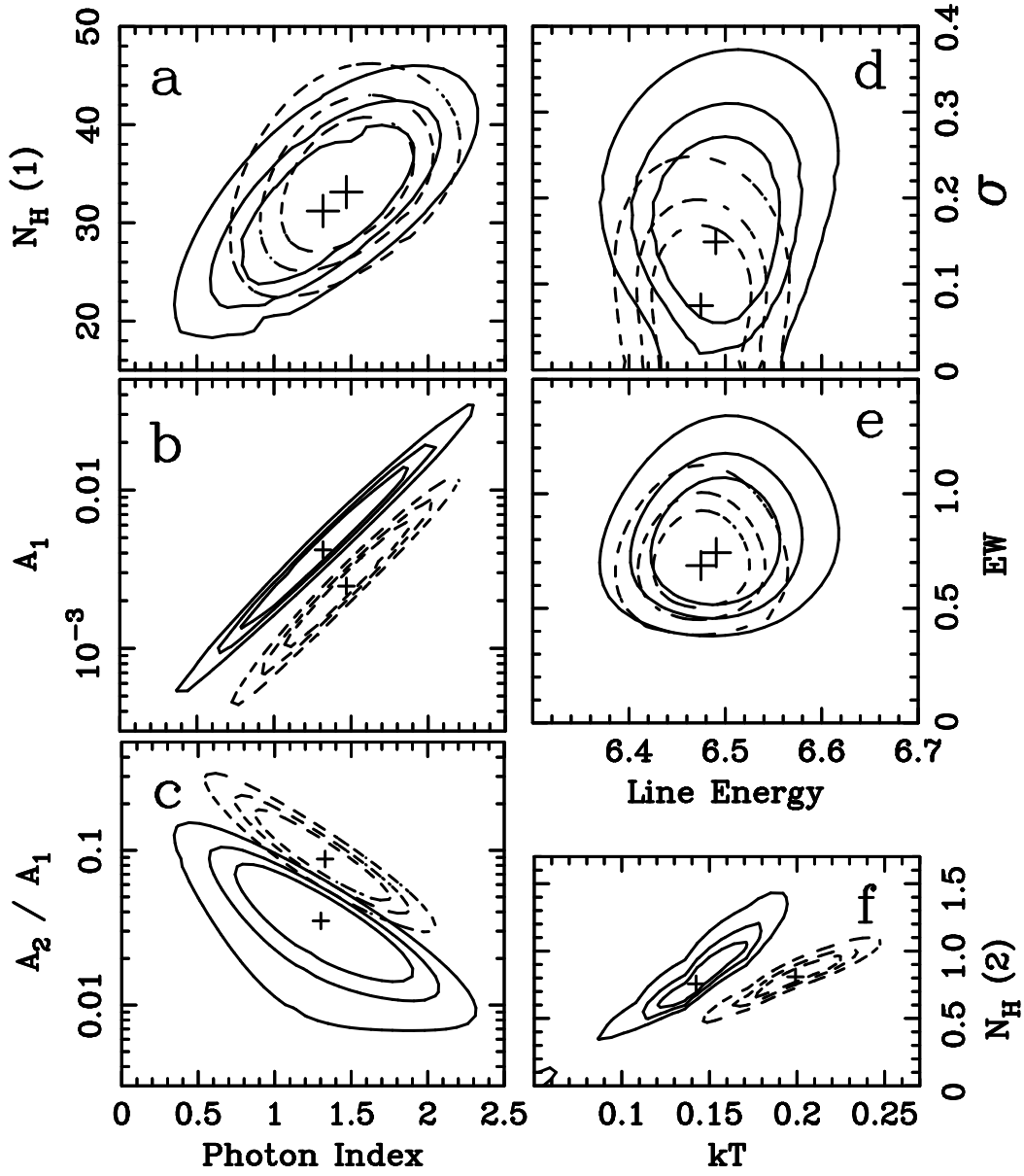


Fig. 4.— Confidence contours for the model parameters of the simultaneous fit to the GIS and SIS *ASCA* spectra of NGC 4388 in 1993 and 1995 (see Table 2a). Contours represent $\Delta\chi^2$ confidence limits (68%, 90%, and 99%) for 4 interesting parameters (IP). *Solid line* – 1993 observation, *dashed line* – 1995 observation. (a) Power law photon index vs. absorbing column (10^{22} cm^{-2}). (b) Power law photon index vs. absorbed power law continuum normalization (photons $\text{cm}^{-2} \text{ s}^{-1} \text{ keV}^{-1}$). (c) Power law photon index vs. ratio of the normalizations of the unabsorbed to absorbed power law continuum (A_2/A_1). (d) Emission line peak energy (keV) vs. emission line width (keV). (e) Emission line peak energy (keV) vs. equivalent width of the line (keV). (f) Temperature of the Raymond-Smith component (keV) vs. second absorbing column (10^{22} cm^{-2}), here the contours are $\Delta\chi^2$ for 2 IP.

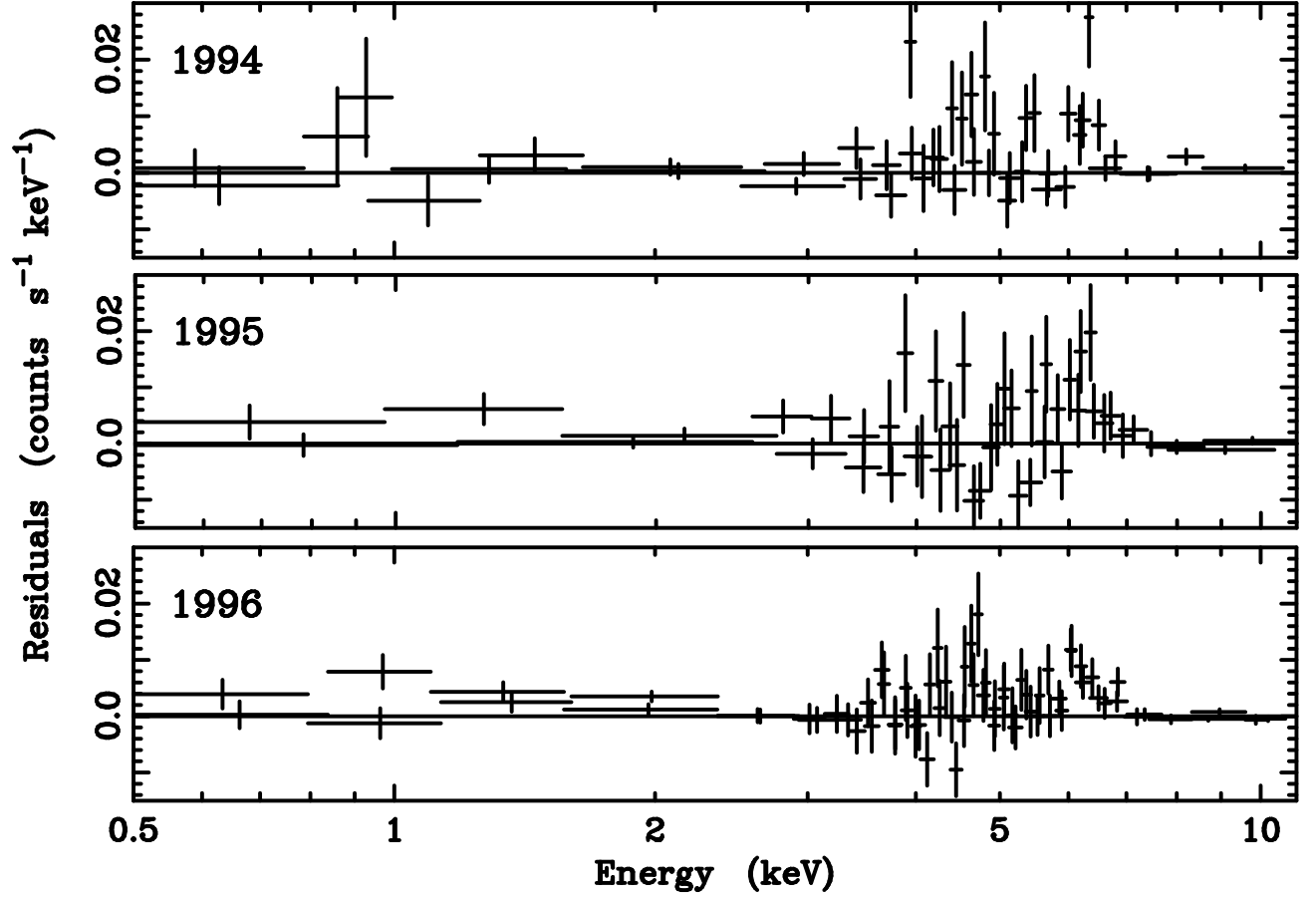


Fig. 5.— Residuals from an absorbed power law continuum model fit to the 1994, 1995, and 1996 *ASCA* spectra of ESO 103–G35. Only the SIS data are shown for clarity.

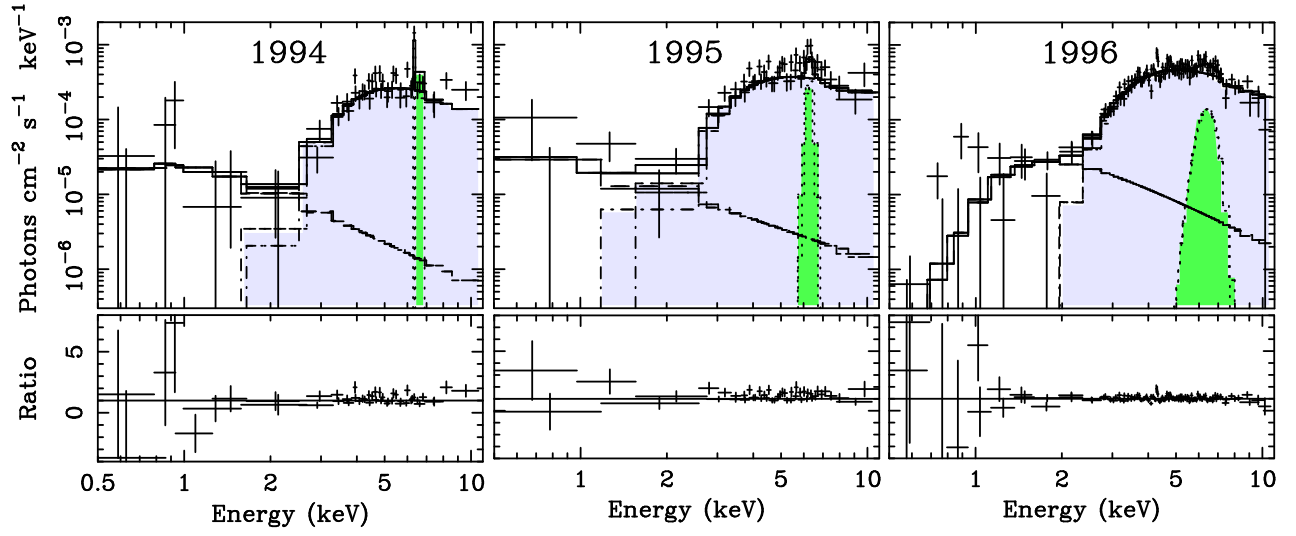


Fig. 6.— *ASCA* spectra of ESO 103-G35 in 1994, 1995, and 1996. Only the SIS data are shown and have been rebinned for clarity. *Top panels* — The data and model unfolded from the instrumental response. The shaded area represents the absorbed power law continuum emission, and the darker shaded region marks the Fe K α emission line. *Bottom panels* — The ratio of the model to the data.

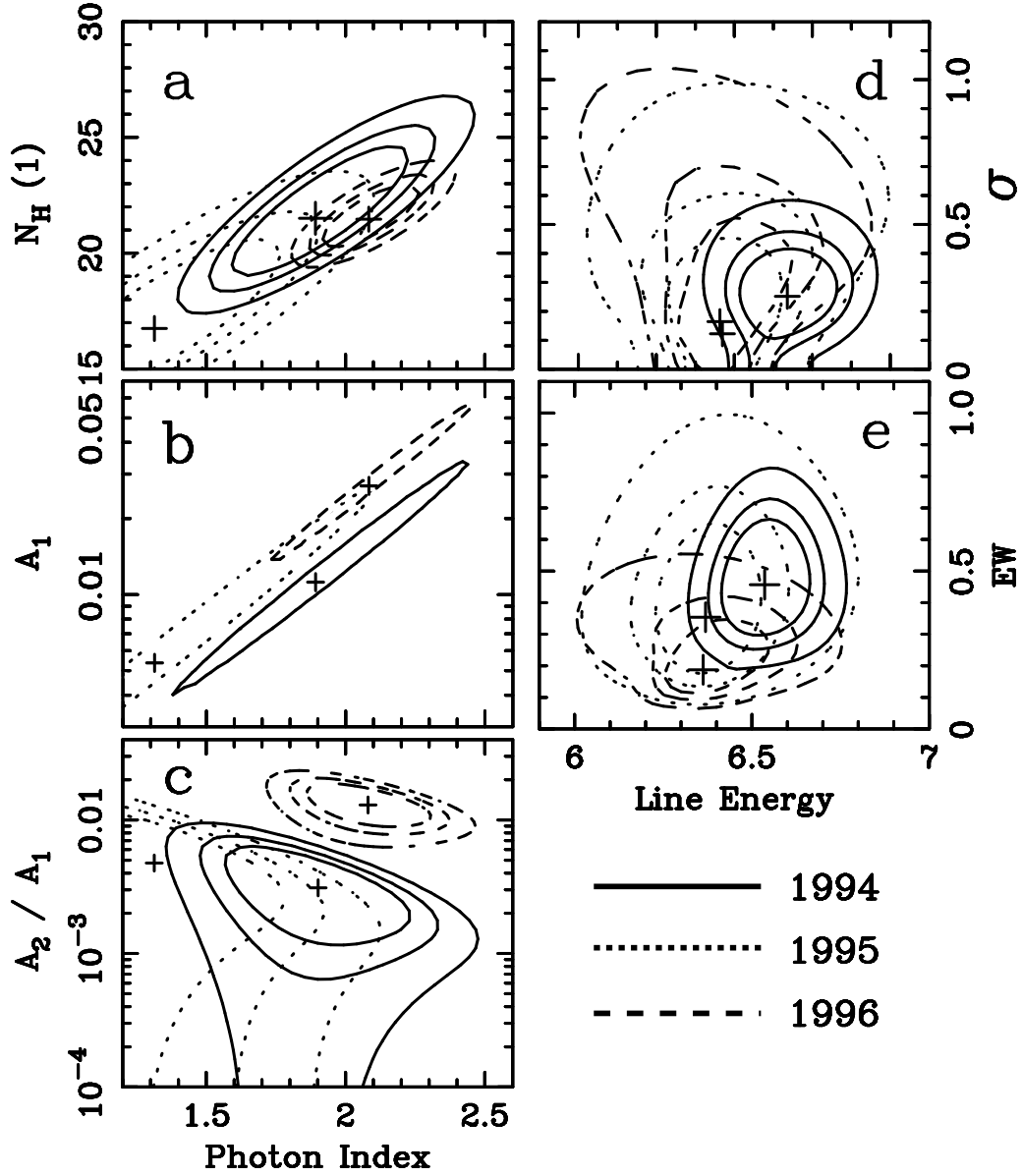


Fig. 7.— Confidence contours for the model parameters of the simultaneous fit to the 1994, 1995 and 1996 *ASCA* GIS and SIS spectra of ESO 103-G35 (see Table 2b). *Solid line* – 1994 observation, *dotted line* – 1995 observation, *dashed line* – 1996 observation. (a – e) See caption for Fig. 4. Note that only the 99% confidence contours are shown in panel b for clarity.

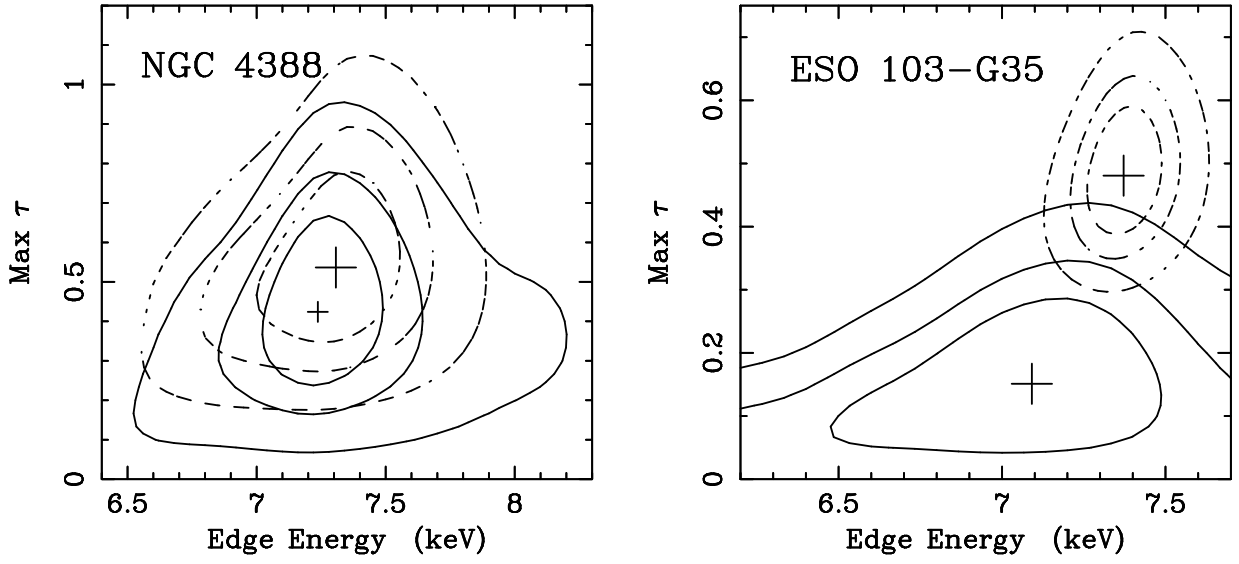


Fig. 8.— Confidence contours for the model parameters of the Fe K absorption edge in the *ASCA* spectra of NGC 4388 and ESO 103-G35. Contours are 68%, 90% and 99% confidence limits for 2 IP. *Solid lines* – 1993/94 observations (NGC 4388/ESO 103-G35). *Dashed lines* – 1995/96 observations. The best fitted value for the 1993 observation of NGC 4388 is represented by a smaller cross.

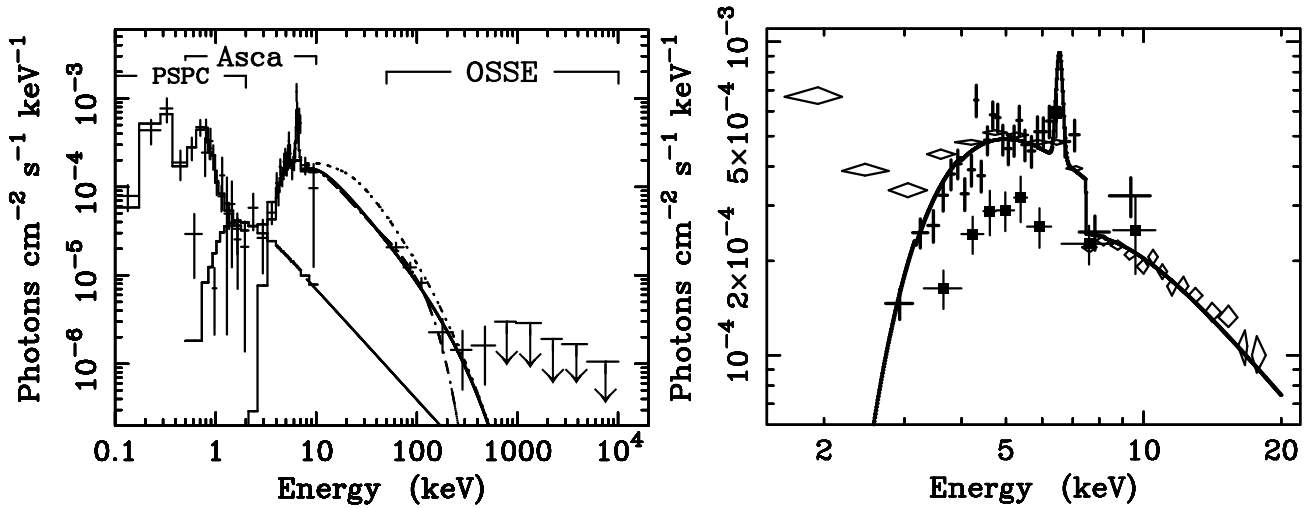


Fig. 9.— *Left* — The X-ray spectrum of NGC 4388 from 0.1 to 10^4 keV. The *ROSAT* PSPC and *ASCA* SIS model (§3.8) is used with an exponential cutoff (solid line) to extend out to the 1993 *CGRO* OSSE observation. The dotted line is a Compton reflection spectrum and the dashed line (lower line) is a thermal Comptonization model. All *ASCA* instruments were modeled simultaneously with the PSPC data, but only the rebinned data from the SIS 0 instrument is shown for clarity. *Right* — The 1988 *Ginga* observation of ESO 103-G35 (diamonds) shown with the 1994 (black square) and 1996 (crosses) *ASCA* SIS 0 observations. The model is that for the *Ginga* observation with an ionized Fe K edge (Warwick et al. 1993). The rise in the *Ginga* spectrum below 3 keV has been attributed to a contaminating soft X-ray source in the field of view of the *Ginga* LAC (Warwick et al. 1993).

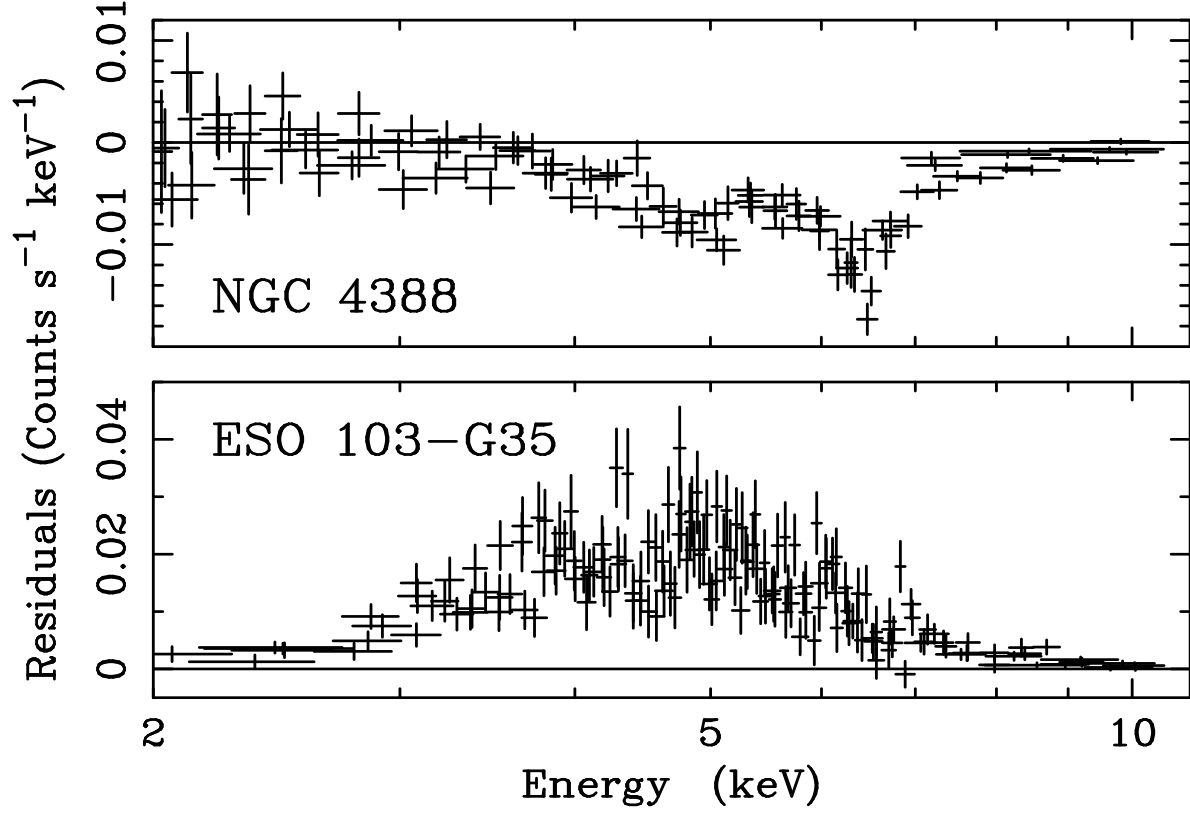


Fig. 10.— Hard X-ray variability of NGC 4388 and ESO 103-G35, both GIS and SIS data are shown. *Top* – The residuals from applying the 1993 model (Table 2a) to the 1995 data of NGC 4388. The variability in the strength of the Fe K α emission line near 6.4 keV can clearly be seen. *Bottom* – As above but applying the 1994 model (Table 2b) to the 1996 data of ESO 103-G35.

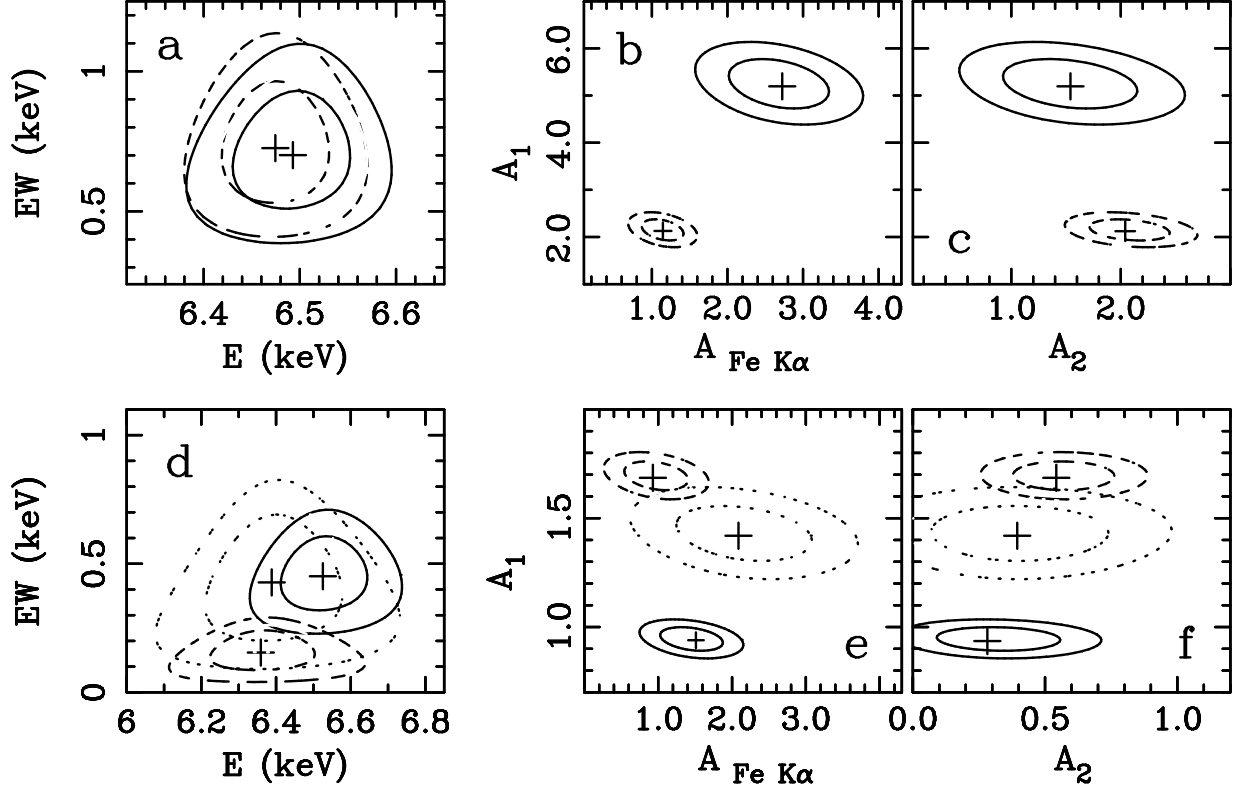


Fig. 11.— The confidence contours of the fixed parameter model in Tables 2a,b. The contours are the 68% and 99% confidence contours for 4 interesting parameters. *Top panels* — NGC 4388, *solid line* = 1993 spectrum, *dashed line* = 1995 spectrum. *Bottom panels* — ESO 103-G35, *solid line* = 1994 spectrum, *dotted line* = 1995 spectrum, *dashed line* = 1996 spectrum. (a,d) Emission line peak energy (keV) vs. emission line equivalent width (keV). (b,e) Total photons held in the emission line (10^{-4} photons $\text{cm}^{-2} \text{s}^{-1}$) vs. normalization of the absorbed power law continuum (10^{-3} (b) 10^{-2} (e) photons $\text{cm}^{-2} \text{s}^{-1} \text{keV}^{-1}$ at 1 keV). (c,f) Normalization of the unabsorbed power law continuum ($A_2 \times 10^{-4}$ photons $\text{cm}^{-2} \text{s}^{-1} \text{keV}^{-1}$ at 1 keV) vs. normalization of the absorbed power law continuum ($A_1 \times 10^{-3}$ photons $\text{cm}^{-2} \text{s}^{-1} \text{keV}^{-1}$ at 1 keV).

TABLE 1a
ASCA OBSERVATIONS OF NGC 4388

Instrument	Date	Exposure ^a (ks)	Count Rate ^b (10 ⁻² s ⁻¹)	Flux ^c (10 ⁻¹¹)	Notes
SIS 0	4 July 1993	14.4	5.01 ± 0.40	1.38	Only 2 CCD mode is used although 4 CCD mode is available. Serendipitous observation in field of view of NGC 4374
SIS 1	13.9	3.68 ± 0.37	
GIS 2	21.2	4.95 ± 0.31	
GIS 3	21.2	3.80 ± 0.30	
SIS 0	21 to 22 June 1995	26.0	5.26 ± 0.28	0.64	Targeted observation in 2 CCD mode
SIS 1	35.7	4.45 ± 0.31	
GIS 2	34.2	3.73 ± 0.24	
GIS 3	27.9	5.12 ± 0.29	
SCREENING CRITERIA ^d					
All data	SAA = 0	COR > 6	ANG_DIST < 0.01	RBM_CONT < 300	
All GIS	G2_L1 > 0.0	G3_L1 > 0.0	ELV > 5		
All SIS	BR_EARTH > 20	ELV > 10			
1993 SIS (2 CCD)	T_SAA > 32	T_DY_NT > 100	S0_PIXL0(2) < 50	S1_PIXL0(2) < 70	
1995 SIS (2 CCD)	T_SAA > 32	T_DY_NT > 100	S0_PIXL0(1) < 80	S1_PIXL0(3) < 100	

TABLE 1b
ASCA OBSERVATIONS OF ESO 103–G35

Instrument	Date	Exposure ^a (ks)	Count Rate ^b (10 ^{−2} s ^{−1})	Flux ^c (10 ^{−11})	Notes
SIS 0	3 to 4 September 1994	11.0	9.19 ± 0.3 0	1.42	2 and 4 CCD modes
SIS 1	6.4	7.23 ± 0.27	
GIS 2	17.2	7.81 ± 0.29	
GIS 3	17.2	10.38 ± 0.32	
SIS 0	26 to 27 September 1995	3.2	13.50 ± 0.71	2.36	1 CCD mode
SIS 1	3.6	11.78 ± 0.63	
GIS 2	3.9	11.02 ± 0.60	
GIS 3	3.9	13.98 ± 0.71	
SIS 0	18 March 1996	15.7	17.31 ± 0.39	2.38	1 CCD Mode
SIS 1	15.5	13.81 ± 0.36	
GIS 2	18.2	13.62 ± 0.34	
GIS 3	18.2	16.72 ± 0.37	

SCREENING CRITERIA ^d

All data	SAA = 0	COR > 6	ANG_DIST < 0.01	RBM_CONT < 200
All GIS	G2_L1 > 0.0	G3_L1 > 0.0	ELV > 5	
All SIS	BR_EARTH > 20	ELV > 10		
1994 SIS (2 CCD)	T_SAA > 32	T_DY_NT > 100	S0_PIXL0(1) < 600	S1_PIXL2(3) < 600
1994 SIS (4 CCD)	T_SAA > 64	T_DY_NT > 200	S0(1)_PIXL0(1,2,3) < 800	
1995 and 1996 SIS (1 CCD)	T_SAA > 16	T_DY_NT > 50	S0_PIXL1 < 80	S1_PIXL3 < 80

^aThe final exposure time after the screening of the data, excluding periods of high background level.

^bBackground subtracted, vignetting corrected count rates for events with $0.5 < E < 10.0$ keV.

^c2.0 to 10.0 keV flux in erg cm^{−2} s^{−1}. The fluxes are for the 2 power law plus Raymond–Smith model (NGC 4388) and the 2 power law model (ESO 103–G35), see Table 2a,b.

^dSAA = South Atlantic Anomaly passage (0 = excluded), COR = Minimum Cut-Off Rigidity (GeV/c), ANG_DIST = rms deviation from mean pointing (degrees), RBM_CONT = Radiation Belt Monitor count threshold, G2(3)_L1 = GIS 2 (3) lower discriminator monitor counts, ELV = Elevation angle between the Earth’s limb and the pointing direction (degrees), BR_EARTH = Angle between the illuminated limb of the Earth and the pointing direction (degrees), T_SAA = Time after passage through SAA (seconds), T_DY_NT = Time after passing through Day-Night terminator (seconds), S0(1)_PIXL0(1,2,3) = SIS 0 (1) chip 0 (1,2,3) event threshold value.

TABLE 2a

NGC 4388 — ASCA GIS AND SIS RAYMOND-SMITH PLUS TWO POWER LAW AND EMISSION LINE MODEL

	Γ	A_1^a (10^{-3})	$E_{\text{FeK}\alpha}$ (keV)	σ (eV)	EW (eV)	N_{H} (1) ^b (10^{23} cm^{-2})	A_2/A_1^c	kT (keV)	Z/Z_{\odot}	N_{H} (2) ^d (10^{21} cm^{-2})	χ^2/dof
1993	$1.32^{+0.77}_{-0.74}$	$4.26^{+4.43}_{-2.16}$	$6.490^{+0.090}_{-0.088}$	150^{+160}_{-130}	750^{+420}_{-300}	$3.15^{+1.11}_{-1.05}$	$0.04^{+0.07}_{-0.03}$	$0.14^{+0.04}_{-0.03}$	$0.13 \leq 4.40$	$7.65^{+2.55}_{-1.25}$	320.6/321
1995	$1.47^{+0.57}_{-0.57}$	$2.52^{+1.44}_{-0.93}$	$6.475^{+0.069}_{-0.067}$	$80 \leq 200$	700^{+320}_{-250}	$3.34^{+0.98}_{-0.84}$	$0.09^{+0.14}_{-0.05}$	$0.20^{+0.04}_{-0.04}$	$0.16^{+1.39}_{-0.11}$	$8.26 \leq 10.25$	542.3/533
1993 ^f	1.41	$5.24^{+0.68}_{-0.66}$	$6.492^{+0.077}_{-0.081}$	120	710^{+290}_{-250}	3.25	0.03 ± 0.02	0.17	0.16	5.4	321.9/327
1995 ^f	1.41	$2.16^{+0.28}_{-0.29}$	$6.474^{+0.071}_{-0.070}$	120	730^{+300}_{-250}	3.25	0.10 ± 0.03	0.17	0.16	5.4	548.7/539

ERRORS: 90% confidence limits for 4 interesting parameters ($\Delta\chi^2 = 7.78$) for all parameters except A_1 , kT and Z/Z_{\odot} where the errors are for 2 interesting parameters ($\Delta\chi^2 = 4.61$). This corresponds to the middle contours in Fig. 4. The relative normalizations of for the GIS and SIS are $A_{\text{SIS}}(1993) = 0.95 A_{\text{GIS}}$ and $A_{\text{SIS}}(1995) = 0.93 A_{\text{GIS}}$.

^aPower law normalization at 1 keV in units of photons $\text{cm}^{-2} \text{ s}^{-1} \text{ keV}^{-1}$.

^bThe column density of the material absorbing the first power law component (A_1).

^cThe ratio of the normalizations for the ‘unabsorbed’ (A_2) and absorbed (A_1) power law components.

^dAll the model components are attenuated by a column of gas with $N_{\text{H}} \geq N_{\text{H}}^{\text{Gal}}$ ($2.54 \times 10^{20} \text{ cm}^{-2}$; Murphy et al. 1996).

^fFixed parameter model, see §3.7.

TABLE 2b
ESO 103-G35 — *ASCA* GIS AND SIS TWO POWER LAW AND EMISSION LINE MODEL

	Γ	A_1^a (10^{-2})	$E_{\text{FeK}\alpha}$ (keV)	σ (eV)	EW (eV)	$N_{\text{H}} (1)^b$ (10^{23} cm^{-2})	A_2/A_1^c (10^{-3})	$N_{\text{H}} (2)$ (10^{22} cm^{-2})	χ^2/dof
1994	$1.89^{+0.35}_{-0.40}$	$1.14^{+1.45}_{-0.30}$	$6.536^{+0.168}_{-0.157}$	$260 \leq 470$	460^{+260}_{-210}	$2.16^{+0.40}_{-0.35}$	$3.17^{+4.42}_{-2.53}$	$0.0764 \leq 1.8$	262.6/275
1995	$1.31^{+0.59}_{-0.57}$	$0.54 \leq 1.40$	$6.370^{+0.232}_{-0.209}$	$130 \leq 610$	360^{+410}_{-230}	$1.68^{+0.54}_{-0.48}$	$4.85 \leq 15.72$	0.0764^d	78.2/93
1996	$2.08^{+0.29}_{-0.28}$	$2.72^{+2.19}_{-1.18}$	$6.363^{+0.270}_{-0.144}$	$170 \leq 710$	200^{+230}_{-110}	$2.16^{+0.26}_{-0.25}$	$13.23^{+7.42}_{-5.47}$	$2.62^{+3.14}_{-1.82}$	534.0/527
1994 ^f	1.81	0.94 ± 0.07	$6.525^{+0.155}_{-0.145}$	200	460^{+190}_{-180}	2.0	$3.43^{+3.17}_{-3.04}$	0.0764^d	267.2/279
1995 ^f	1.81	1.43 ± 0.16	$6.388^{+0.200}_{-0.188}$	200	440^{+170}_{-250}	2.0	$2.81 \leq 5.91$	0.0764	83.4/97
1996 ^f	1.81	1.69 ± 0.08	$6.360^{+0.181}_{-0.170}$	200	160^{+100}_{-90}	2.0	$3.37^{+1.41}_{-1.43}$	0.0764	560.3/531

ERRORS: 90% confidence limits for 4 interesting parameters ($\Delta\chi^2 = 7.78$), this corresponds to the middle contours in Fig. 7.

The relative normalizations for the GIS and SIS are $A_{\text{SIS}} (1994) = 1.00 A_{\text{GIS}}$, $A_{\text{SIS}} (1995) = 1.13 A_{\text{GIS}}$ and $A_{\text{SIS}} (1996) = 1.08 A_{\text{GIS}}$.

^aPower law normalization at 1 keV in units of photons $\text{cm}^{-2} \text{ s}^{-1} \text{ keV}^{-1}$.

^bThe column density of the material absorbing the first power law component (A_1).

^cThe ratio of the normalizations of the ‘unabsorbed’ (A_2) and absorbed (A_1) power law components.

^dAll the model components are attenuated by a column of gas with $N_{\text{H}} \geq N_{\text{H}}^{\text{Gal}}$ ($7.64 \times 10^{20} \text{ cm}^{-2}$; Stark et al. 1992).

^fFixed parameter model, see §3.7.

TABLE 3
THE DUAL ABSORPTION MODEL FOR THE *ASCA* SPECTRA
OF NGC 4388 ^a

	Γ	N_{H} (1) (10^{23} cm^{-2})	CF ^b	N_{H} (2) (10^{23} cm^{-2})	χ^2/dof ^c
1993	$1.89^{+0.35}_{-0.36}$	$9.7^{+3.5}_{-2.0}$	$0.71^{+0.05}_{-0.04}$	$3.12^{+0.45}_{-0.38}$	320.3/319
1995	$1.84^{+0.26}_{-0.22}$	$4.5^{+1.5}_{-1.1}$	$0.70^{+0.09}_{-0.01}$	$2.36^{+0.48}_{-0.39}$	540.5/531

ERRORS are $\Delta\chi^2 = 90\%$ for 2 interesting parameters.

^aThis model includes 3 absorbing columns, a Raymond–Smith thermal component, 2 Power law continua and a Gaussian emission line near 6.4 keV. The parameters for the emission line and the thermal component are identical to those given in Table 2a.

^bCovering factor of the larger absorbing column (1).

^c χ^2/dof is for the model that includes 3 absorbing columns, a Raymond–Smith thermal component, 2 power law continua and a gaussian emission line near 6.4 keV.